American Mineralogist, Volume 68, pages 880–899, 1983

Titanium, aluminum and interlayer cation substitutions in biotite from high-grade gneisses, West Greenland

ROBERT F. DYMEK

Department of Geological Sciences
Harvard University, Cambridge, Massachusetts 02138

Abstract

A detailed electron microprobe study has been carried out on biotite in pelitic to mafic metamorphic rocks from two localities in West Greenland. Comparison of analyses from similar rock types indicates higher Ti, K/(K+Na), and possibly (K+Na), similar Al^{IV}, and lower Al^{VI} in granulite *vs.* amphibolite grade samples. Normalization of the analyses on the basis of 7 octahedral and tetrahedral cations results in calculated total positive charge that exceeds the theoretical maximum of 22.0 in all cases, assuming an anion framework of 10 oxygen and 2(OH+F+Cl). In granulite grade biotite this charge excess correlates well with 2Ti, indicating that vacancy- or oxy-substitution [$Ti^{4+} + \square = 2R^{2+}$ or $Ti^{4+} + 2O^{2-} = R^{2+} + 2(OH)^-$] predominate over ones in which octahedral Ti is balanced by tetrahedral Al. The vacancy substitution is preferred as the best explanation of these data. Many analyses yield a charge excess above that accounted for by Ti, and contain Al^{VI} not balanced by Al^{IV}. In amphibolite grade biotite, charge excess correlates with 3/2 Al^{VI}, suggesting additional vacancies associated with dioctohedral substitution [$2Al^{3+} + \square = 3R^{2+}$]. Vacancy-formation does not appear to violate any crystal–chemical relationships in biotite, and may be necessary to accommodate substitution of the smaller Al and Ti for Fe and Mg in octahedral positions.

These results lead to an iterative normalization procedure for microprobe analyses of biotite [Total Cations − (K+Na+Ca+Ba) + Ti + ½Al^{VI}_{xc} = 7.0, where $Al^{VI}_{xc} = (Al+Cr)^{VI} - Al^{IV} + (K+Na+2Ca+2Ba)$], which allocates a vacancy for each Ti and 2 Al^{VI}_{xc}. This iterative normalization eliminates charge excess, and permits Fe^{3+} to be estimated (exclusive of oxyannite).

A model chemical system for micas is discussed which illustrates how many complex substitutional mechanisms can be reduced to linear combinations of four simple types [Tschermak: MgSi = AlAl; Dioctohedral: 3Mg = 2Al□; Ti-spinel: MgTi = 2Al; Talc: □Si = KAl]. On the basis of these relationships, a method is described for recasting biotite microprobe analyses into selected end-members.

Introduction

The composition of biotite can deviate considerably from the theoretical range of the phlogopite–annite series: $K^A(Mg,Fe^{2+})^{VI}(Si_3Al)^{IV}O_{10}(OH)_2$. The most common cation substitutions involve replacement of Mg^{2+} and Fe^{2+} by Al^{3+}, Fe^{3+} and Ti^{4+} on octahedral sites, and Si^{4+} by additional Al^{3+} on tetrahedral sites. In some situations, replacement of K by Na on the interlayer or "A" site may also be important.

Biotite crystal chemistry is complicated further by the apparent occurrence of vacancies. Foster (1960a,b) demonstrated rather convincingly that octahedral occupancy in biotite is generally less than 3 cations/formula. Similarly, many recalculated biotite analyses yield A-site occupancies less than 1.

The presence of these "other" cations causes a distortion of the biotite structure due to differences in ionic radius and charge (*e.g.*, Hazen and Wones, 1972), and may exert a strong influence on both the stability range of biotite (Rutherford, 1973; Forbes and Flower, 1974; Hewitt and Wones, 1975; Robert, 1976a,b), and on Mg–Fe partitioning between biotite and other silicates such as muscovite (Guidotti *et al.*, 1977) and garnet (Dahl, 1969; Dallmeyer, 1974a). In addition, Goldman and Albee (1977) discussed some effects that Ti- and Al-substitution could have on biotite–garnet geothermometry.

The effects of possible vacancies on biotite stability are unclear, but in all probability are linked to the nature of the cation(s) with which they are associated (*cf.*, Forbes and Flower, 1974). More important, however, are the problems posed for calculations of mineral equilibria involving a complex solid solution phase like biotite, since extrapolations of experimental and/or thermodynamic data obtained on simple systems to "rock" sys-

0003–004X/83/0910–0880$02.00

tems require certain assumptions about how cation substitutions proceed (Holdaway and Lee, 1977; Holdaway, 1980). Consequently, it is important to examine in detail possible substitutional mechanisms for the above-mentioned cations through a consideration of their dependence on host rock composition and mineral assemblage, and where metamorphic rocks are concerned, their dependence on metamorphic grade.

This paper presents the results of a detailed microprobe study on biotites occurring in high-grade schists and gneisses from West Greenland, which will be used to evaluate certain features of Ti-, Al- and A-site substitutions. Selected groups of analyzed biotites in metamorphic rocks from other areas are also examined in an attempt to apply the generalities deduced from the Greenland samples. Biotites from associations such as granitoid igneous rocks, ultramafic rocks, *etc.*, are not considered here, but will be dealt with separately at a later date.

Summary of cation substitutions

This section outlines some general aspects of chemical substitutions in biotite that are relevant to the present study. It is not intended to be a comprehensive review of this subject, but rather to establish a framework for data presentation and discussion that follows.

The dominant mechanism causing Al-enrichment in biotite involves the Al-Tschermak's substitution:

$$(R^{2+})^{VI} + (Si^{4+})^{IV} = (Al^{3+})^{VI} + (Al^{3+})^{IV}, \qquad (1)$$

which relates phlogopite–annite to the aluminous end-member eastonite $[KMg_2AlSi_2Al_2O_{10}(OH)_2]$.[1] Previous studies have shown that the amount of Al-Tschermak substitution appears to increase slightly up to sillimanite zone, and perhaps decrease at still higher grade (Tracy and Robinson, 1978). At a given P and T, it is maximized in biotite that coexists with an Al-saturating phase such as staurolite, sillimanite, *etc.*

Foster (1960a,b) showed that many biotite analyses yielded Al^{VI} that could not be accommodated by substitution (1). She suggested that this additional Al is incorporated in biotite by means of a dioctohedral-trioctohedral substitution:[2]

$$3(R^{2+})^{VI} = 2(Al^{3+})^{VI} + (\square)^{VI}, \qquad (2)$$

which could be viewed as a muscovite component in biotite, and results in the formation of octahedral vacancies. Rutherford (1973) indicated that substitution (2) occurs only to a limited extent (10–12%) in the Mg-free system, although observations on natural biotites suggest that dioctohedral substitution is maximized in a biotite coexisting with muscovite, a situation not realized in Rutherford's experiments.

Ti-substitution in biotite is problematic. Kunitz (1936) suggested that Ti^{4+} replaces Si^{4+} on tetrahedral sites, and some recent studies of biotites from kimberlites and mantle xenoliths, where $\Sigma(Si+Al) < 4$, provide some support for this idea. When this tetrahedral Si–Al "deficiency" was first recognized, Fe^{3+} was assigned to fill the tetrahedral sites (*e.g.*, Dawson and Smith, 1977; Delaney *et al.*, 1980). However, Farmer and Boettcher (1981) have shown that $(Fe^{3+})^{IV}$ is most plausibly associated with only those biotites that display reverse pleochroism (*cf.*, Faye and Hogarth, 1969), which also have $\Sigma(Si+Al+Ti) < 4$. Farmer and Boettcher (1981) conclude that Ti^{4+} may enter tetrahedral sites in those biotites with normal pleochroism, and $\Sigma(Si+Al) < 4$.

Engel and Engel (1960) suggested that Ti^{3+} replaces Al^{3+} on octahedral sites. Studies of the optical spectra of biotite, however, reveal absorption bands interpreted to indicate Fe^{2+}–Ti^{4+} intervalence charge transfer, and are ambiguous in regard to Ti^{3+} (Faye, 1968; Burns and Vaughan, 1975). In contrast, Evans and Raftery (1980), based on an X-ray photoelectron diffraction study, concluded that Ti is trivalent in the biotites which they investigated (assemblages unspecified). It is unclear what implications this result has for the present study, where nearly all biotites coexist with a Ti^{4+} oxide (ilmenite or rutile). The position taken here is that Ti occurs as $(Ti^{4+})^{VI}$, which is the prevailing opinion of most workers.

Ti^{4+}-substitution on VI-fold sites is complicated by its high charge and small cation radius (0.605Å) compared to Mg^{2+} (0.72Å) and Fe^{2+}(0.78Å) (ionic radii from Shannon, 1976). Several substitutional mechanisms have been suggested for Ti^{4+} in biotite. The first involves a coupled VI- and IV-fold relationship:

$$(R^{2+})^{VI} + 2(Si^{4+})^{IV} = (Ti^{4+})^{VI} + 2(Al^{3+})^{IV}. \qquad (3)$$

Substitution (3) can be viewed as a Ti-Tschermak's component (analogous to $R^{2+}TiAl_2O_6$ in pyroxene) leading to the theoretical end-member Ti-eastonite $[KMg_2TiSiAl_3O_{10}(OH)_2]$, and was favored by Czamanske and Wones (1973), Robert (1976a,b), Guidotti *et al.* (1977) and Tracy (1978). A second coupled substitution would be:

$$(Al^{3+})^{VI} + (Si^{4+})^{IV} = (Ti^{4+})^{VI} + (Al^{3+})^{IV}. \qquad (4)$$

Direct substitution of Ti for Al on octahedral sites may occur in two ways:

$$2(Al^{3+})^{VI} = (Ti^{4+})^{VI} + (R^{2+})^{VI}, \text{ and} \qquad (5)$$

$$2(R^{2+})^{VI} = (Ti^{4+})^{VI} + (\square)^{VI}. \qquad (6)$$

[1] The formula as listed is more aluminous than what is typically referred to as eastonite in the literature, but is used here for convenience. The existence of natural end-member eastonite is problematic. Strunz (1970) noted that the original material was probably a phlogopite–vermiculite intergrowth, whereas Foster (1960b) had previously drawn attention to this situation. An analysis by the writer (unpublished) on a sample from the "type" locality (Easton, PA; Philadelphia Academy #26550) shows it to be nearly pure phlogopite with ~4.6 wt.% F.

[2] Foster (1960a,b) actually considered $(R^{3+})^{VI}$. Substitution (2) thus represents a simplification of her results; $(Fe^{3+})^{VI}$ is considered separately here.

Substitution (5) can be viewed as a Ti-spinel component, whereas (6) results in the formation of octahedral vacancies; the latter was favored by Dahl (1969), Forbes and Flower (1974), and Dymek and Albee (1977). The final Ti-substitution involves a dehydrogenation reaction:

$$(R^{2+})^{VI} + 2(OH)^- = (Ti^{4+})^{VI} + 2(O^{2-}) + H_2, \quad (7)$$

leading to anhydrous end-member Ti-oxybiotite [$KMg_2TiSi_3AlO_{12}$].

Clearly, there is no consensus as to the nature of Ti-substitution(s) in biotite, and recently Bohlen *et al.* (1980), and Abrecht and Hewitt (1980, 1981) have indicated that combinations of (3), (6) and (7) are necessary to explain their data. Whatever the case, observations on natural biotite indicate that Ti-content is maximized where biotite coexists with a Ti-saturating oxide phase, and that Ti-content increases with increasing metamorphic grade (*e.g.*, Kwak, 1968; Guidotti *et al.*, 1977).

In a limited number of cases, $(Fe^{3+})^{IV}$ is assigned from structural formula calculations (*cf.*, Foster, 1960a,b; Czamanske and Wones, 1973). However, as mentioned above, the presence of tetrahedral Fe^{3+} may be revealed by reverse pleochroism, and both synthetic and natural ferri-annite [$KFe^{2+}_3Si_3Fe^{3+}O_{10}(OH)_2$] show this feature (Wones, 1963a; Miyano and Miyano, 1982).

Fe^{3+} in octahedral coordination may proxy for Al^{3+} via a Ferri-Tschermak's substitution:

$$(R^{2+})^{VI} + (Si^{4+})^{IV} = (Fe^{3+})^{VI} + (Al^{3+})^{IV}, \quad (8)$$

yielding the end-member ferri-eastonite with composition [$KMg_2Fe^{3+}Si_2Al_2O_{10}(OH)_2$]. This substitution should be maximized where biotite coexists with an Fe^{3+}-saturating phase such as magnetite or hematite.

An additional, important mechanism relevant to Fe^{3+} in biotite involves *in situ* oxidation of Fe^{2+} as represented by the following reaction:

$$Fe^{2+} + (OH)^- = Fe^{3+} + O^{2-} + \tfrac{1}{2}H_2. \quad (9)$$

Many aspects of the resulting oxy-annite end-member [$KFe^{2+}Fe^{3+}_2Si_3AlO_{12}$] were discussed by Eugster and Wones (1962) and Wones and Eugster (1965), and Wones (1963b) showed that Reaction (9) was entirely reversible upon hydrogenation, and that Fe^{2+}/Fe^{3+} in biotite was therefore strongly dependent upon f_{H_2}.

Chemical variations on the A site in biotite may arise from at least two sources. Substitution of H_3O^+ for K^+ could explain a low abundance of interlayer cations and/or high water contents found in some mica analyses. Alternatively, a low abundance of interlayer cations could result from the following substitution:

$$(K^+)^A + (Al^{3+})^{IV} = (\square)^A + (Si^{4+})^{IV}, \quad (10)$$

which relates phlogopite–annite to a talc component [$\square^A(Mg,Fe^{2+})_3Si_4O_{10}(OH)_2$], and would represent a potassic analogue to the edenite substitution in amphibole. Similarly, K–Na substitution would relate phlogopite to its Na-counterpart, which was synthesized by Carman (1974), and recognized recently as a new mineral (wonesite) in schists from Vermont (Spear *et al.*, 1978, 1981). In addition, the Na-counterpart to eastonite has also been identified (preiswerkite; Keusen and Peters, 1980).

Normalization procedures

Electron microanalysis cannot distinguish between Fe^{2+} and Fe^{3+}, and H_2O is likewise not determined with the microprobe. Consequently, calculations of formula proportions from analyses of a hydrous, Fe^{3+}-bearing mineral such as biotite requires certain assumptions.

Two normalization schemes are commonly applied. The first can be expressed by the relationship:

$$\text{Total Cations} - (K+Na+Ca+Ba) = 7.0, \quad (A)$$

which assumes complete occupancy of octahedral and tetrahedral sites (*cf.*, Ludington and Munoz, 1975). Such "cation-based" normalization procedures are unaffected by the valence state of iron and variations in H_2O-content, and can be exceedingly useful since they permit a straightforward estimation of Fe^{3+}-contents in many silicates and oxides (*e.g.*, pyroxene, garnet, spinel, ilmenite, and probably amphibole). In biotite, assuming a full complement of 10 oxygen and 2 (OH,F,Cl) per formula unit, Fe^{3+} would be equal to the difference between 22.0 and the calculated total positive charge. However, if octahedral vacancies are present [*e.g.*, substitutions (2) and (6)], formula proportions calculated from (A) will be overestimated in direct proportion to the number of vacancies, and a corresponding calculated charge excess would result, which, among other things, makes Fe^{3+}-estimates impossible. Alternatively, a charge excess may not be indicative of vacancies, but may be compensated by an oxygen excess related to the occurrence of oxycomponents [*e.g.*, substitution (7)[3]].

The second scheme, which assumes that all iron occurs as Fe^{2+}, involves normalization to 11 oxygen atoms expressed by the following relationship:

$$\text{Total Cation Charge} = 22.0. \quad (B)$$

This procedure is unaffected by vacancies, but causes cation abundances to be overestimated in direct proportion to the number of Fe^{3+} cations that are present, which remains an unknown quantity. However, if there is an oxygen excess (*i.e.*, oxycomponents), total charge $\neq$ 22.0, and calculated formula proportions are underestimated.

Some investigators (*e.g.*, Czamanske and Wones, 1973) have used a modified form of (B) by applying a fixed Fe^{2+}/Fe^{3+} ratio to their biotite data based on partial wet chemical analyses. In the general case where information

[3] Because the initial charge calculation is made with all iron as Fe^{2+}, a charge excess at this point cannot be due to oxyannite substitution.

of this type is lacking, normalization of biotite microprobe analyses involves a tradeoff between assumption of no vacancies and no Fe^{3+}. In a subsequent section of this paper, an iterative normalization procedure is presented that bypasses these assumptions, and permits an Fe^{3+}-estimate to be made.

Samples studied

The results reported in this paper comprise part of an ongoing investigation of the mineralogy and petrology of the Archaean (>3000 Ma) Malene supracrustals, a series of sedimentary and volcanic rocks from the Godthåb District, West Greenland, which were subjected to intense regional metamorphism at *ca.* 2800 Ma (*cf.*, Dymek, 1978). Biotite in samples from two localities at different grades of metamorphism are considered. The first locality (Langø; 64°52′N, 52°12′W) was metamorphosed under granulite grade conditions (Sill–Kf zone; ~7.5 kbar, 750°C). Three lithologies are distinguished:[4] a. Potassium feldspar gneisses (Bio + Kf + Plag + Qtz ± Garn ± Crd ± Sill ± Ilm); b. Orthopyroxene gneisses (Bio + Plag + Qtz + Opx ± Garn ± Crd ± Sill ± Ilm/Rut ± Mag); c. Pyribolite (Bio + Plag + Hbl + Opx + Cpx ± Mag ± Ilm).

The biotite content of these samples ranges from ~1 to 20 volume percent. Many of the samples contain biotite grains with different colors and textures, indicating at least two episodes of mineral growth. Only primary biotite, which is brown and Ti-rich (up to 6 wt.% TiO_2), is considered here.

Most samples contain a Ti-saturating phase, which is typically ilmenite, with rutile restricted to the most Mg-rich assemblages. Magnetite, representing Fe^{3+}-saturation, is common in pyribolites. Quartz is abundant (≥5 vol%) in all samples except pyribolites, in which it is typically absent. Sillimanite occurs in about half of the potassium feldspar gneisses and in a few orthopyroxene gneisses. In all diagrams presented herein, sillimanite-bearing potassium feldspar gneisses are distinguished from sillimanite-free types. Plagioclase occurs in all samples.

The second locality (Itivdlinguaq = Itiv; 64°13′N, 51°31′W) was metamorphosed at amphibolite grade conditions (Stl-Sill zone, ~5.5 kbar, 575°C). Three lithologies are distinguished here also: a. Muscovite schist (Bio + Musc + Plag + Qtz + Sill ± Stl + Ilm); b. Semipelitic schist (Bio + Plag + Qtz ± Crd ± Garn ± Oamph ± Stl ± Sill + Ilm or Rut); c. Amphibolite (Bio + Plag + Qtz ± Hbl ± Cumm ± Oamph ± Garn + Ilm). The biotite content of these samples ranges from ~1 to 25 volume percent. As in samples from Langø, there are two generations of biotite at Itiv, but only primary biotite is considered. These are green, with TiO_2-contents in the range 0.7–2.3 wt.%.

All samples studied from Itiv contain quartz, plagioclase, and a Ti-saturating phase (either ilmenite or rutile). Sillimanite occurs in muscovite schists and in a few of the semipelitic schists.

Although regional correlation of lithologies is imprecise in the Godthåb District, the rocks from Langø are believed to be higher grade equivalents of those from Itiv, and the following comparisons can be made: muscovite schist → sillimanitic Kf gneiss; semipelitic schist → orthopyroxene gneiss; amphibolite → pyribolite.

In summary, the approach adopted here is that by studying a large number of samples of differing bulk compositions, a more thorough understanding of the range of possible biotite compositions at a given metamorphic grade will be achieved. Thus, it should be possible to discriminate between grade-dependent and grade-independent substitutions. This contrasts with the approach that focuses on a specific rock composition and examines biotites in only limiting (or nearly so) assemblages. In the latter kinds of rocks, the extent of all cation substitutions is fixed by P, T, and volatile activities, and compositional variation at a given metamorphic grade is precluded by the choice of samples.

Results

General compositional characteristics

A representative analysis from each sample studied is listed in Tables 1–6, where they are grouped by lithologic type. A description of analytical techniques is provided in the Appendix.

Individual biotite analyses are illustrated in Figure 1 in terms of relative amounts of MgO, FeO_T+MnO, and Al_2O_3. All analyses are enriched in Al_2O_3 compared to phlogopite–annite, and span a large range of Mg-value [=Mg/(Mg+Fe+Mn)]. The much greater range of Mg-values found in the granulite-grade samples from Langø compared to those in amphibolite-grade samples from Itiv is probably related to the rock compositions studied. Although there is no apparent difference in the overall relative concentration of Al_2O_3 in biotite from the two localities, the Al-content is related to the nature of the rock type in which it occurs, reflecting a trend towards Al-saturation. In samples from Langø, the Al-content increases in the order pyribolite → orthopyroxene gneiss → Kf-gneiss. In the latter group, sillimanite-bearing samples are clearly distinguished from sillimanite-free samples. In samples from Itiv, the Al-content increases in the order amphibolite → semipelitic schist → muscovite schist. The most Al-rich biotite in semipelitic schists occurs in sillimanite-bearing samples.

With the exception of the above-mentioned Al-enrichment, and high TiO_2-contents (up to ~6 wt.%), the compositions of the biotites are relatively simple. The amounts of Na_2O (<0.7 wt.%), MnO (<0.4 wt.%), and ZnO (<0.2 wt.%) are low; CaO was generally not detected, whereas Cl was near the limits of detection in most cases; F-contents are also low, although values as high as ~1 wt.% were found. Routine analyses were not performed for Cr_2O_3 and BaO, but reconnaissance work indicates low concentrations (<0.2 and <0.4 wt.% each). In summary, the analyses presented here appear similar to ones reported from high-grade metamorphic rocks by other investigators.

[4] In this paper the following abbreviations are used: Bio = biotite; Kf = potassium feldspar; Plag = plagioclase; Qtz = quartz; Garn = garnet; Crd = cordierite; Sill = sillimanite; Ilm = ilmenite; Rut = rutile; Mag = magnetite; Opx = orthopyroxene; Hbl = hornblende; Cpx = clinopyroxene; Musc = muscovite; Stl = staurolite; Oamph = orthoamphibole; Cumm = cummingtonite.

Table 1. Microprobe analyses of biotite in potassium feldspar and sillimanite–potassium feldspar gneisses, Langø.

Wt %	1.	2.	3.	4.	5.	6.	7.
SiO_2	37.20	36.80	36.45	36.71	36.28	36.25	36.77
Al_2O_3	18.64	18.81	18.16	16.42	16.57	16.18	15.79
TiO_2	2.27	2.25	3.17	3.42	3.65	3.80	4.85
MgO	16.37	13.93	13.12	11.04	10.87	12.12	13.78
FeO_T	11.02	14.12	15.31	17.72	18.51	16.96	15.50
MnO	0.09	0.07	0.01	0.09	0.18	0.07	0.17
ZnO	0.00	0.13	0.00	0.16	0.11	0.20	0.00
CaO	0.02	0.00	0.00	0.00	0.00	0.00	0.00
Na_2O	0.07	0.00	0.04	0.04	0.00	0.02	0.03
K_2O	9.77	10.03	10.13	9.68	9.85	9.73	9.61
F	0.27	0.21	0.23	0.34	0.60	0.43	0.10
Cl	0.03	0.01	0.01	0.48	0.01	0.01	0.01
Total*	96.15	96.27	96.53	95.85	96.38	95.59	96.57

FORMULA PROPORTIONS**

IV	Si	2.776	2.732	2.758	2.710	2.755	2.697	2.851	2.779	2.807	2.742	2.799	2.740	2.777	2.722
	Al	1.224	1.268	1.242	1.290	1.245	1.303	1.149	1.221	1.193	1.258	1.201	1.260	1.223	1.278
VI	Al	0.394	0.325	0.420	0.343	0.373	0.281	0.355	0.245	0.318	0.218	0.272	0.182	0.183	0.101
	Ti	0.126	0.124	0.127	0.125	0.180	0.176	0.200	0.195	0.212	0.208	0.221	0.216	0.276	0.270
	Mg	1.796	1.768	1.556	1.529	1.478	1.447	1.279	1.246	1.254	1.225	1.395	1.366	1.552	1.521
	Fe	0.678	0.668	0.885	0.870	0.968	0.948	1.151	1.122	1.198	1.170	1.096	1.072	0.979	0.960
	Mn	0.006	0.006	0.004	0.004	0.001	0.001	0.006	0.006	0.012	0.012	0.005	0.004	0.011	0.011
	Zn	0.000	0.000	0.007	0.007	0.000	0.000	0.009	0.009	0.006	0.006	0.011	0.011	0.000	0.000
	Σ	3.000	2.890	3.000	2.878	3.000	2.853	3.000	2.823	3.000	2.838	3.000	2.852	3.000	2.862
A	Ca	0.002	0.002	0.000	0.000	0.000	0.000	0.000	0.000	0.000	0.000	0.000	0.000	0.000	0.000
	Na	0.010	0.010	0.000	0.000	0.006	0.006	0.006	0.006	0.000	0.000	0.003	0.003	0.004	0.004
	K	0.917	0.903	0.959	0.942	0.977	0.956	0.959	0.935	0.972	0.950	0.959	0.938	0.926	0.908
	Σ	0.929	0.914	0.959	0.942	0.983	0.962	0.965	0.941	0.972	0.950	0.962	0.941	0.930	0.912

* *1. OGA-24c Qtz-Plag-Kf-Sill-Garn-Ilm (22.352†) 2. OGA-24d Qtz-Plag-Kf-Sill-Garn-Ilm (22.390) 3. OGA-36h-1 Qtz-Plag-Kf-Sill-Kf-Garn-Ilm (22.471) 4. OGA-29 Qtz-Plag-Kf-Ilm/Mt (22.572) 5. OGA-27 Qtz-Plag-Kf-Ilm (22.521) 6. OGA-25e Qtz-Plag-Kf-Ilm (22.475) 7. OGA-36b Qtz-Plag-Kf-Ilm-Opx (?) (22.441)*

** Minus oxygen for F, Cl ** Based on 7 cations (1st column) and 11 oxygens (2nd column)*
† Numbers in parentheses correspond to calculated total positive charge for the 7 cation normalization

Ti-substitution

Ti- and Al^{IV}-contents of the biotite are illustrated in Figure 2, with formula proportions based on the 11 oxygen normalization (B). Biotite in the amphibolite and granulite grade samples have a similar range of Al^{IV}, but the latter contain substantially higher Ti.

If all Ti^{VI} and Al^{IV} were balanced by substitution (3), then the data points should lie along the lines labeled 1/2. Any data falling below this line could be interpreted as resulting from the combined effects of the Al- and Ti-Tschermak's substitutions [(1) and (3)].

All but three of the analyses of biotite from Itiv lie below the ½ line, which is a necessary but not sufficient condition for supporting the above interpretation. However, the majority of the Langø analyses contain Ti that is impossible to balance by Al^{IV}, thereby requiring an additional (or different) Ti-substitutional mechanism. If one were to attribute this "extra" Ti to an overestimation of cation abundances due to an unknown amount of Fe^{3+} in each analysis, the situation would not change dramatically. For example, recalculating the most Fe- and Ti-rich analyses with all iron as Fe^{3+} increases Al^{IV} by a maximum of 0.12 and decreases Ti by 0.02.

Figure 3a demonstrates that a remarkably good correlation exists between calculated total positive charge and Ti-content in biotite from Langø, with formula proportions based on the 7 cation normalization scheme (A). Note that the data points scatter about the line labeled Charge Excess = 2 Ti, which was not constructed to fit the data, but is merely a line drawn from zero Ti-content with a slope of 2.[5] This relationship between charge excess and Ti-content suggests that substitutions (3), (4) and (5) play a subordinate role for Ti-substitution in these biotites, since they involve the same number of cations with the same net charge. However, the data in Figure 3a are consistent with either the Ti-vacancy (6) or Ti-oxy (7)

[5] The fact that the charge excess correlates with 2Ti strongly suggests the presence of Ti^{4+} rather than Ti^{3+}.

Table 2. Microprobe analyses of biotite in orthopyroxene gneisses, Langø.

Wt %	1.	2.	3.	4.	5.	6.	7.	8.
SiO_2	37.82	37.57	38.50	37.91	39.04	37.91	37.35	37.02
Al_2O_3	16.89	17.14	16.45	16.30	15.66	16.57	16.70	17.30
Cr_2O_3	n.a.	0.00	n.a.	n.a.	n.a.	0.04	0.06	n.a.
TiO_2	1.39	1.42	2.26	2.64	2.75	2.77	3.04	3.39
MgO	18.96	19.29	20.25	17.91	20.71	18.43	17.54	16.23
FeO_T	10.31	9.13	7.64	11.27	7.95	10.39	10.54	10.96
MnO	0.00	0.02	0.10	0.03	0.00	0.04	0.02	0.05
ZnO	0.01	0.00	0.16	0.00	0.09	0.00	0.00	0.00
CaO	0.00	0.02	0.00	0.01	0.00	0.00	0.00	0.00
BaO	n.a.	0.23	n.a.	n.a.	n.a.	0.18	0.38	n.a.
Na_2O	0.00	0.03	0.09	0.22	0.25	0.05	0.22	0.02
K_2O	10.11	9.30	10.00	9.49	9.13	9.60	9.47	10.29
F	0.32	n.a.	0.42	0.31	0.28	n.a.	n.a.	0.28
Cl	0.01	n.a.	0.01	0.01	0.04	n.a.	n.a.	0.03
Total*	95.68	94.15	95.70	96.03	95.77	95.98	95.32	95.45

FORMULA PROPORTIONS**

IV	Si	2.767	2.756	2.761	2.754	2.796	2.773	2.783	2.759	2.812	2.796	2.771	2.747	2.771	2.734	2.775	2.720
	Al	1.233	1.244	1.239	1.246	1.204	1.227	1.217	1.241	1.188	1.204	1.229	1.253	1.229	1.266	1.225	1.280
VI	Al	0.224	0.207	0.246	0.235	0.205	0.169	0.200	0.162	0.143	0.119	0.199	0.163	0.231	0.175	0.304	0.218
	Cr	-	-	0.000	0.000	-	-	-	-	-	-	0.002	0.002	0.004	0.003	-	-
	Ti	0.077	0.076	0.079	0.078	0.123	0.122	0.146	0.145	0.149	0.148	0.152	0.151	0.170	0.167	0.191	0.187
	Mg	2.068	2.060	2.113	2.108	2.193	2.174	1.961	1.943	2.224	2.212	2.009	1.991	1.940	1.914	1.814	1.778
	Fe	0.631	0.628	0.561	0.560	0.464	0.460	0.692	0.686	0.479	0.476	0.635	0.630	0.654	0.645	0.687	0.674
	Mn	0.000	0.000	0.001	0.001	0.006	0.006	0.002	0.002	0.000	0.000	0.002	0.002	0.001	0.001	0.003	0.003
	Zn	0.001	0.001	0.000	0.000	0.009	0.009	0.000	0.000	0.005	0.005	0.000	0.000	0.000	0.000	0.000	0.000
	Σ	3.000	2.972	3.000	2.982	3.000	2.941	3.000	2.938	3.000	2.960	3.000	2.940	3.000	2.907	3.000	2.860
A	Ca	0.000	0.000	0.002	0.002	0.000	0.000	0.001	0.001	0.000	0.000	0.000	0.000	0.000	0.000	0.000	0.000
	Ba	-	-	0.007	0.007	-	-	-	-	-	-	0.005	0.005	0.011	0.011	-	-
	Na	0.000	0.000	0.004	0.004	0.013	0.013	0.031	0.031	0.035	0.035	0.007	0.007	0.032	0.032	0.003	0.003
	K	0.944	0.940	0.872	0.871	0.927	0.919	0.889	0.881	0.839	0.834	0.895	0.888	0.896	0.884	0.984	0.964
	Σ	0.944	0.940	0.884	0.883	0.939	0.931	0.921	0.913	0.874	0.869	0.907	0.900	0.939	0.927	0.987	0.967

1. OGA-28d Qtz-Plag-Opx-Mt (22.087†) 2. GRD-1441 Qtz-Plag-Garn-Opx-Mt (22.056) 3. GGU-35861,2 Qtz-Plag-Opx-Cord-Rut (22.187) 4. OGA-28h Qtz-Plag-Opx-Cord-Sill-Rut (22.196) 5. OGA-28b Qtz-Plag-Opx-Cord-Rut (22.147) 6. GRD-1447 Qtz-Plag-Garn-Cord-Opx-Sill-Ilm (22.190) 7. Grd-1439 Qtz-Plag-Garn-Opx-Ilm (22.295) 8. GGU-35861,1 Qtz-Plag-Cord-Opx-Sill-Rut (22.449)

** Minus oxygen for F, Cl ** Based on 7 cations (1st column) and 11 oxygens (2nd column) n.a. = not analyzed*
† Numbers in parentheses correspond to calculated total positive charge based on the 7 cation normalization

substitutions, as both lead to excess positive charge using normalization procedure (A). The relationship between calculated positive charge and Ti-content in biotite from Itiv (Fig. 3b) is more complicated than that for Langø. This apparent difference is related to the Al-content, and will be discussed in the next section.

The total positive charge used in Figure 3 is calculated assuming that all iron is Fe^{2+}. If, in fact, some of the iron is Fe^{3+}, then the positive charge is higher and the charge excess greater. The net result of the assumption of all ferrous iron is that data points plot lower on the positive charge axis than they otherwise would if the amount of ferric iron were known beforehand. Hence, the value for positive charge represents a minimum value.[6] In Figure 3a, nearly all analyses of biotite from pyribolites, which contain magnetite and are therefore Fe^{3+}-saturated, plot below the line. This lowered positive charge is consistent with the presence of Fe^{3+} in these analyses. However, nearly all of the analyses of biotite from potassium feldspar gneisses plot above the line, and more than half of the analyses from Itiv plot above the line as well (Fig. 3b). Thus a majority of the biotite analyses have a charge excess which exceeds that accounted for by Ti-substitution.

Al-substitution

Biotite compositions are illustrated in Figures 4a and 4b in terms of Al^{VI} and Al^{IV} with formula proportions based on the 7 cation normalization (A). If the substitution of Al^{VI} into biotite occurred only by the Al-Tschermak's component (1), then the data points should fall along the lines labeled $Al^{VI} = Al^{IV}$. The presence of a Ferri-Tschermak's component (8) should result in Al^{IV} exceeding Al^{VI} in direct proportion to the amount of $(Fe^{3+})^{VI}$.

[6] A slight note of caution should be added here due to the lack of Li_2O-determinations. However, the Li-abundances observed to occur in most "common" biotites are typically very low. Unless the Greenland biotites are anomalous, inclusion of Li in the charge calculations will not change the observed relationships in a significant way.

Table 3. Microprobe analyses of biotite in pyribolites, Langø.

Wt %	1.	2.	3.	4.	5.	6.	7.	8.
SiO_2	38.89	37.86	39.07	37.44	36.94	36.41	37.32	37.81
Al_2O_3	15.23	14.60	13.92	14.91	14.56	14.86	14.39	14.23
TiO_2	2.48	3.24	3.44	4.50	5.13	5.28	5.34	5.63
MgO	20.43	17.68	18.62	15.72	13.76	13.24	14.55	15.95
FeO_T	7.36	12.83	10.79	13.05	15.09	15.99	14.81	11.91
MnO	0.03	0.04	0.00	0.13	0.05	0.03	0.04	0.07
ZnO	0.00	0.12	0.00	0.02	0.20	0.13	0.07	0.08
CaO	0.00	0.00	0.00	0.00	0.00	0.00	0.00	0.00
Na_2O	0.25	0.12	0.12	0.02	0.12	0.02	0.02	0.04
K_2O	9.85	9.75	9.36	9.77	9.78	9.60	10.15	9.89
F	0.50	0.35	0.09	0.55	0.07	0.14	0.31	0.10
Cl	0.01	0.02	0.03	0.01	0.06	0.02	0.02	0.00
Total*	94.82	96.46	95.40	95.89	95.72	95.66	96.87	95.67
FORMULA PROPORTIONS**								
IV Si	2.855 2.822	2.798 2.777	2.883 2.850	2.822 2.769	2.832 2.764	2.796 2.735	2.825 2.759	2.856 2.783
Al	1.145 1.178	1.202 1.223	1.117 1.150	1.178 1.231	1.168 1.236	1.204 1.265	1.175 1.241	1.144 1.217
VI Al	0.173 0.124	0.070 0.040	0.094 0.047	0.146 0.069	0.149 0.048	0.142 0.051	0.109 0.013	0.123 0.017
Ti	0.137 0.135	0.180 0.179	0.191 0.189	0.255 0.250	0.290 0.289	0.305 0.298	0.304 0.297	0.320 0.312
Mg	2.236 2.210	1.948 1.934	2.049 2.025	1.766 1.733	1.573 1.535	1.516 1.483	1.642 1.604	1.796 1.750
Fe	0.452 0.447	0.793 0.787	0.666 0.658	0.823 0.807	0.968 0.944	1.027 1.005	0.938 0.916	0.752 0.733
Mn	0.002 0.002	0.003 0.002	0.000 0.000	0.008 0.008	0.003 0.003	0.002 0.002	0.003 0.003	0.004 0.004
Zn	0.000 0.000	0.007 0.007	0.000 0.000	0.001 0.001	0.011 0.011	0.007 0.007	0.004 0.004	0.004 0.004
Σ	3.000 2.918	3.000 2.948	3.000 2.919	3.000 2.869	3.000 2.830	3.000 2.847	3.000 2.837	3.000 2.821
A Ca	0.000 0.000	0.000 0.000	0.000 0.000	0.000 0.000	0.000 0.000	0.000 0.000	0.000 0.000	0.000 0.000
Na	0.036 0.036	0.017 0.017	0.017 0.017	0.003 0.003	0.018 0.017	0.003 0.003	0.003 0.003	0.006 0.006
K	0.923 0.912	0.919 0.912	0.881 0.871	0.939 0.922	0.957 0.933	0.941 0.920	0.980 0.957	0.953 0.929
Σ	0.959 0.948	0.936 0.929	0.898 0.888	0.942 0.925	0.975 0.951	0.944 0.923	0.983 0.960	0.959 0.934

1. OGA-23b Plag-Hbl-Opx-Cpx-Ilm/Mt (22.260†) 2. OGA-38b Qtz-Plag-Hbl-Cpx-Ilm/Mt = Nordnor metadiorite (22.164) 3. OGA-35b Plag-Hbl-Opx-Cpx-Ilm/Mt (22.258) 4. OGA-24e Qtz-Plag-Hbl-Opx-Cpx-Ilm/Mt (22.421) 5. OGA-25d Qtz-Plag-Hbl-Cpx-Ilm/Mt (22.547) 6. OGA-36k Qtz-Plag-Hbl-Opx-Cpx-Ilm/Mt (22.492) 7. OGA-37 Qtz-Plag-Hbl-Opx-Cpx-Ilm/Mt = Nordnor metadiorite (22.526) 8. OGA-34a Qtz-Plag-Opx-Ilm/Mt (22.577).

**Minus oxygen for F,Cl **Based on 7 cations (1st column) and 11 oxygens (2nd column)*
† Numbers in parentheses correspond to calculated total positive charge for the 7 cation normalization

Table 4. Microprobe analyses of biotite in muscovite schists, Itivdlinguaq.

Wt %	1.	2.
SiO_2	36.95	36.20
Al_2O_3	18.75	19.95
TiO_2	1.45	1.35
MgO	13.46	11.49
FeO_T	15.61	16.55
MnO	0.26	0.34
ZnO	0.04	0.02
CaO	0.00	0.00
Na_2O	0.27	0.19
K_2O	9.12	9.71
F	0.26	0.96
Cl	0.06	0.02
Total*	96.11	96.37

FORMULA PROPORTIONS**		1.	2.
IV	Si	2.766 2.733	2.754 2.702
	Al	1.234 1.267	1.246 1.298
VI	Al	0.420 0.369	0.543 0.458
	Ti	0.082 0.081	0.077 0.076
	Mg	1.502 1.485	1.303 1.279
	Fe	0.977 0.966	1.053 1.033
	Mn	0.016 0.016	0.022 0.022
	Zn	0.002 0.002	0.001 0.001
	Σ	3.000 2.919	3.000 2.868
A	Ca	0.000 0.000	0.000 0.000
	Na	0.039 0.039	0.028 0.028
	K	0.871 0.861	0.942 0.925
	Σ	0.910 0.899	0.970 0.953

1. OGA-48Q Qtz-Plag-Musc-Stl-Ilm (22.422†)
2. GGU-91691 Qtz-Plag-Musc-Stl-Sill-Ilm-Gahn (22.259)

** Minus oxygen for F, Cl ** Based on 7 cations (1st column) and 11 oxygens (2nd column)*
† Numbers in parentheses correspond to calculated total positive charge for the 7 cation normalization

All biotite analyses from Itiv and the majority of analyses from Langø, however, plot above the $Al^{VI} = Al^{IV}$ line, indicating the presence of Al^{VI} not balanced by Al^{IV}. If $(Fe^{3+})^{VI}$ from (8) were added to Al^{VI}, the $(R^{3+})^{VI}$ excess would be even larger (*cf.*, Foster, 1960a, b).

The relationships shown in Figure 4 can be correlated with those in Figure 3 to the extent that most of the analyses which contain excess or "uncompensated" Al^{VI} also yield a calculated positive charge that lies above the lines in Figure 3. Although it could be argued that the features discussed in Figure 4 are an artifact of the 7 cation normalization (A), when the data are portrayed in terms of the 11 oxygen normalization (B), a similar Al^{VI}-excess remains.

Calculated total positive charge is plotted versus Al^{VI} in Figure 5. No trend is apparent in the data from Langø, although analyses from the different lithologies fall into distinct fields, once again reflecting the trend towards Al-saturation in the sillimanite-bearing samples. The data from Itiv, with the exception of biotite analyses in hornblende-bearing samples, appear to define a trend in which positive charge excess is proportional to 3/2 Al^{VI}. This is exactly the relationship that is expected if the incorpo-

Table 5. Microprobe analyses of biotite in semipelitic schists, Itivdlinguaq.

Wt %	1.	2.	3.	4.	5.	6.	7.	8.	9.	10.
SiO_2	39.38	38.75	37.67	37.49	36.51	38.16	37.43	36.67	37.40	36.91
Al_2O_3	17.74	17.68	16.90	18.04	18.27	17.89	18.54	18.90	17.73	18.43
TiO_2	0.71	0.91	1.04	1.16	1.22	1.25	1.29	1.30	1.32	1.48
MgO	19.08	18.68	16.99	14.91	14.61	15.04	14.88	14.49	14.74	13.35
FeO_T	10.23	10.18	12.90	15.66	16.02	14.51	15.16	15.19	15.71	17.27
MnO	0.05	0.01	0.02	0.06	0.00	0.00	0.00	0.00	0.00	0.02
ZnO	0.00	0.00	0.00	0.02	0.00	0.05	0.10	0.15	0.00	0.00
CaO	0.00	0.00	0.00	0.00	0.00	0.00	0.00	0.00	0.00	0.00
Na_2O	0.67	0.68	0.64	0.46	0.38	0.48	0.51	0.47	0.45	0.50
K_2O	8.52	8.30	8.26	8.33	9.18	8.55	8.45	9.40	8.58	8.96
F	0.71	0.36	0.42	0.11	0.42	0.40	0.17	0.34	0.10	0.16
Cl	0.03	0.02	0.04	0.02	0.02	0.01	0.02	0.02	0.01	0.01
Total*	96.81	95.41	94.69	96.21	96.45	96.17	96.47	96.78	96.00	97.02
					FORMULA PROPORTIONS**					
IV Si	2.816 2.807	2.806 2.796	2.790 2.784	2.762 2.753	2.714 2.703	2.818 2.792	2.752 2.737	2.720 2.696	2.773 2.758	2.745 2.721
Al	1.184 1.193	1.194 1.204	1.210 1.216	1.238 1.247	1.286 1.297	1.182 1.208	1.248 1.263	1.280 1.304	1.227 1.242	1.255 1.279
VI Al	0.312 0.298	0.316 0.300	0.266 0.257	0.328 0.315	0.316 0.298	0.376 0.333	0.359 0.336	0.374 0.335	0.323 0.299	0.361 0.323
Ti	0.038 0.038	0.050 0.049	0.058 0.058	0.064 0.064	0.068 0.068	0.069 0.069	0.071 0.071	0.073 0.072	0.074 0.073	0.083 0.082
Mg	2.035 2.028	2.017 2.009	1.876 1.872	1.638 1.633	1.619 1.613	1.656 1.641	1.631 1.622	1.603 1.589	1.629 1.621	1.480 1.467
Fe	0.612 0.610	0.617 0.614	0.799 0.798	0.965 0.962	0.996 0.992	0.896 0.888	0.932 0.927	0.943 0.934	0.974 0.969	1.074 1.065
Mn	0.003 0.003	0.001 0.001	0.001 0.001	0.004 0.004	0.000 0.000	0.000 0.000	0.000 0.000	0.000 0.000	0.000 0.000	0.001 0.001
Zn	0.000 0.000	0.000 0.000	0.000 0.000	0.001 0.001	0.000 0.000	0.003 0.003	0.005 0.005	0.008 0.008	0.000 0.000	0.000 0.000
Σ	3.000 2.976	3.000 2.973	3.000 2.986	3.000 2.979	3.000 2.871	3.000 2.935	3.000 2.962	3.000 2.938	3.000 2.962	3.000 2.939
A Ca	0.000 0.000	0.000 0.000	0.000 0.000	0.000 0.000	0.000 0.000	0.000 0.000	0.000 0.000	0.000 0.000	0.000 0.000	0.000 0.000
Na	0.093 0.093	0.096 0.095	0.092 0.092	0.066 0.066	0.055 0.055	0.069 0.068	0.073 0.072	0.068 0.067	0.065 0.064	0.072 0.071
K	0.777 0.775	0.767 0.764	0.780 0.779	0.783 0.780	0.871 0.867	0.806 0.798	0.793 0.788	0.890 0.882	0.812 0.807	0.850 0.842
Σ	0.870 0.867	0.862 0.859	0.872 0.871	0.849 0.846	0.926 0.922	0.875 0.866	0.865 0.861	0.957 0.949	0.876 0.872	0.922 0.914

1. OGA-48h Qtz-Plag-Stl-Crd-Oamph-Ilm (22.075†) 2. OGA-48g Qtz-Plag-Stl-Crd-Oamph-Ilm (22.084) 3. OGA-48k Qtz-Plag-Stl-Crd-Garn- Oamph-Rut-Ilm (22.044)
4. OGA-48e Qtz-Plag-Crd-Gar-Ilm (22.067) 5. OGA-48t-3,1 Qtz-Plag-Stl-Gar-Sill-Ilm (22.092) 6. OGA-48r-2 Qtz-Plag-Stl-Gar-Oamph- Ilm (22.207)
7. OGA-48j Qtz-Plag-Stl-Gar-Ilm (22.120) 8. OGA-48t-1 Qtz-Plag-Gar-Sill-Ilm (22.197) 9. OGA-48l Qtz-Plag-Stl-Gar-Oamph-Ilm (22.119)
10. OGA-48t-3,2 Qtz-Plag-Stl-Crd-Garn-Ilm (22.194)

** Minus oxygen for F, Cl ** Based on 7 cations (1st column) and 11 oxygens (2nd column)*
† Numbers in italics correspond to total positive charge caluculated for the 7 cation normalization.

ration of large amounts of Al^{VI} in biotite occurs by means of the vacancy-forming dioctohedral substitution (2). In addition, the relationship between positive charge and Al^{VI} in the Itiv data (Fig. 5b) provides an explanation for the apparent lack of correlation between positive charge and Ti in these analyses (Fig. 3b). Thus, the relationships between calculated positive charge, Ti and Al^{VI} reflect the fact that Ti-substitution dominates charge excess in the granulite grade biotite (Langø; Figs. 3a and 5a), whereas Al^{VI}-substitution dominates the charge excess in the amphibolite grade biotite (Itiv; Figs. 3b and 5b).

A geometric consideration

In principal, it should be possible to devise a graphical method for evaluating the problem of Ti- and Al-substitution that is independent of normalization. Figure 6 is a representation of mica compositions that uses molecular percentages of the oxides as its basis. The corners S ($=SiO_2+2K_2O+2Na_2O+2BaO+2CaO$), Fm ($=FeO_T+MgO+MnO+ZnO-TiO_2$) and A ($=2Al_2O_3+2Cr_2O_3+2TiO_2-2K_2O-2Na_2O-2BaO-2CaO$) were selected so that the compositional fields for all possible dioctahedral and trioctahedral micas are clearly separated as shown. In addition, since phlogopite, eastonite and Ti-eastonite are colinear, substitution of a Ti-Tschermak's component is readily distinguishable from other Ti-substitutions. Thus, only substitution of a Ti-oxycomponent (7) or the vacancy components [(2) and (6)] can shift data points off the phlogopite–eastonite join towards the S corner.

The analyses of the Greenland biotites, recalculated in S-FM-A coordinates, are illustrated in Figure 7 (which is an expanded portion of the trioctahedral mica field shown in Figure 6), where it can be seen that nearly all analyses are displaced from the phlogopite–eastonite join. Although one could argue that the positions of the data points are related solely to substitution of a muscovite component, this does not appear to be the case. In particular, the analyses of biotite from pyribolites, which are the most Ti-rich but have the lowest Al^{VI}-contents (*cf.*, Fig. 4a), extend furthest from the phlogopite–eastonite join. These relationships indicate that a Ti-Tschermak's component is unimportant here, but this diagram does not allow for a distinction between Ti-vacancy and Ti-oxy substitutions.

A-site substitution

The K-contents of biotite from Langø and Itiv range from 0.82–0.98 and 0.73–0.95 cations/formula respectively, whereas Na-contents range up to 0.04 and 0.11 cations/formula. The use of normalization (A) or (B) does not change these values significantly.

These data are summarized in Figure 8, which illustrates $(Na+K+Ba+Ca)^A$ and Al^{IV} based on the 11 oxygen normalization (B), and shows that all analyses lie

Table 6. Microprobe analyses of biotite from amphibolites, Itivdlinguaq.

Wt %	1.	2.	3.	4.	5.	6.
SiO_2	37.76	38.04	37.43	38.39	36.44	36.37
Al_2O_3	17.45	17.34	17.16	16.68	16.64	16.26
TiO_2	1.33	1.36	1.54	1.39	1.73	2.22
MgO	14.96	15.18	14.19	14.01	11.83	11.35
FeO_T	15.10	14.40	15.19	16.06	19.82	19.68
MnO	0.00	0.00	0.01	0.06	0.16	0.12
ZnO	0.01	0.09	0.00	0.00	0.00	0.00
CaO	0.00	0.00	0.00	0.00	0.00	0.00
Na_2O	0.36	0.29	0.29	0.26	0.15	0.13
K_2O	8.82	8.72	8.39	9.00	9.33	9.44
F	0.24	0.20	0.34	0.13	0.05	0.02
Cl	0.02	0.01	0.03	0.06	0.01	0.01
Total*	96.00	95.54	94.42	95.97	96.14	95.59

FORMULA PROPORTIONS**

IV	Si	2.802	2.781	2.825	2.801	2.827	2.800	2.875	2.839	2.781	2.757	2.807	2.769
	Al	1.198	1.219	1.175	1.199	1.173	1.200	1.125	1.161	1.219	1.243	1.193	1.231
VI	Al	0.329	0.296	0.344	0.307	0.355	0.314	0.348	0.294	0.279	0.242	0.287	0.229
	Ti	0.074	0.074	0.076	0.075	0.088	0.087	0.078	0.077	0.099	0.098	0.129	0.127
	Mg	1.655	1.643	1.681	1.667	1.598	1.583	1.564	1.545	1.346	1.335	1.306	1.288
	Fe	0.941	0.934	0.895	0.887	0.960	0.951	1.006	0.994	1.265	1.255	1.271	1.253
	Mn	0.000	0.000	0.000	0.000	0.001	0.001	0.004	0.004	0.010	0.010	0.008	0.008
	Zn	0.001	0.001	0.005	0.005	0.000	0.000	0.000	0.000	0.000	0.000	0.000	0.000
	Σ	3.000	2.947	3.000	2.940	3.000	2.935	3.000	2.913	3.000	2.940	3.000	2.906
A	Ca	0.000	0.000	0.000	0.000	0.000	0.000	0.000	0.000	0.000	0.000	0.000	0.000
	Na	0.052	0.051	0.042	0.041	0.042	0.042	0.038	0.037	0.022	0.022	0.019	0.019
	K	0.835	0.829	0.826	0.819	0.808	0.801	0.860	0.849	0.909	0.901	0.930	0.917
	Σ	0.887	0.880	0.868	0.861	0.851	0.843	0.898	0.886	0.931	0.923	0.949	0.936

1. OGA-48ab Qtz-Plag-Garn-Cumm-Oamph-Ilm (22.166†) 2. OGA-48u Qtz-Plag-Cumm-Oamph-Hbl-Ilm (22.189)
3. OGA-48z Qtz-Plag-Garn-Cumm-Hbl-Ilm (22.207) 4. GGU-91722 Qtz-Plag-Hbl-Cumm-Ilm (22.277)
5. OGA-48y Qtz-Plag-Hbl-Garn-Ilm (22.189) 6. OGA-48a Qtz-Plag-Hbl-Ilm 22.300)

**Minus oxygen for F, Cl **Based on 7 cations (1st column) and 11 oxygens (2nd column)*
†Numbers in parentheses correspond to calculated total positive charge for the 7 cation normalization

within the field bounded by talc–phlogopite–eastonite. There is no major distinction between the two sets of data, although analyses from Itiv extend to lower values of A-site occupancy. The possibility that A-site occupancy increases with metamorphic grade was suggested by Holdaway (1980), and the data presented here are not inconsistent with that interpretation. In addition, the data in Figure 8 suggest substitution of up to ~20% of a talc component (10), and a study of biotite in talc-bearing rocks is in progress to investigate this problem further.

The "composition" of the A-site shows a definite grade-dependent variation. As illustrated in Figure 9, granulite grade biotite (Langø) is characterized by higher K/(K+Na) compared to amphibolite grade biotite (Itiv). Analyses from the three lithologies under consideration display a similar shift towards higher K-contents in the granulite grade samples, making a bulk composition control appear unlikely. If these data are in fact reflecting a grade dependent phenomenon, then they suggest a higher thermal stability for the K end-member. Alternatively, the data could be reflecting a crystal–chemical effect in which high Ti-content precludes substantial substitution of the smaller Na for K. Additional discussion of this point is presented in the following section.

Discussion

Previous studies of biotite have established the complex nature of cation substitutions in that mineral, but the precise mechanisms for several of these remain uncertain. The data on Greenland biotites presented in the previous section extend the observations made by other investigators, and indicate that their contents of Al and Ti, as well as the composition of their A site, change from amphibolite to granulite grade, and are systematically related to rock composition and mineral assemblage. In addition, these new data suggest that Ti-Tschermak's substitution is subordinate in these biotites, but the data are consistent with either Ti-vacancy or Ti-oxy substitution. Additional vacancy substitution is suggested by the presence of Al^{VI} not balanced by Al^{IV}.

In this section, the chemical data for the Greenland biotites are summarized along with data from other

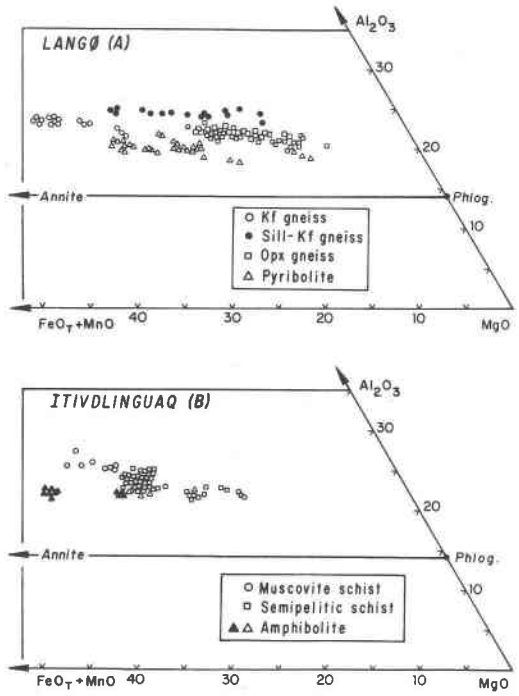

Fig. 1. Composition of granulite grade biotite from Langø (a) and amphibolite grade biotite from Itivdlinguaq (b) illustrated in terms of relative concentrations of MgO, Al_2O_3 and FeO_T + MnO. In (b), analyses marked with the solid symbol (▲) contain hornblende as the dominant amphibole; these analyses are also distinguished in subsequent figures.

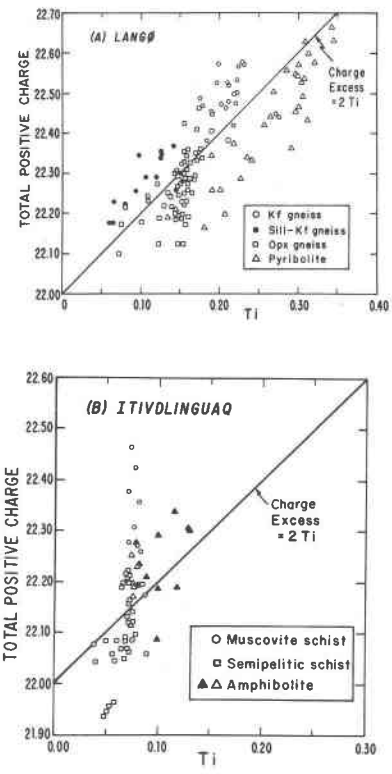

Fig. 3. Calculated total positive charge and Ti-content in biotite from Langø (a) and Itivdlinguaq (b), with formula proportions based on the 7 cation normalization (A).

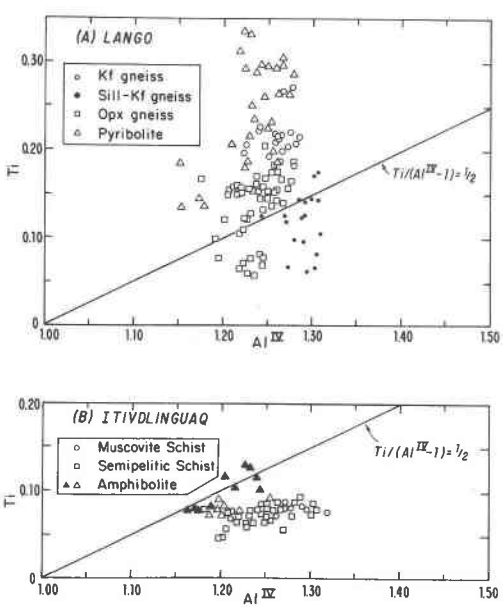

Fig. 2. Ti- and Al^{IV}-contents of biotite from West Greenland with formula proportions based on the 11 oxygen normalization (B).

sources in an attempt to resolve this ambiguity of vacancy *vs.* oxy substitution. Thereafter, an iterative normalization procedure is presented, which utilizes the conclusions deduced from the cation substitutions, and permits Fe^{3+}-estimates to be made from microprobe analyses of biotite. In addition, a model system is presented that discusses the interrelationships among the various cation substitutional mechanisms, on the basis of which biotite analyses can be recast into selected end-members. Finally, the implications of the data are explored with respect to biotite crystal chemistry. The discussion begins, however, with an examination of biotite in metamorphic rocks from selected other localities following the same general methods as for the Greenland biotites.

Comparison with other data

Several sets of electron microprobe analyses of metamorphic biotite are considered in this section to determine whether the observations on Ti- and Al-substitution described above have more widespread applicability. These data sets include biotite from the following associations: metagraywacke and metapelite from a contact aureole, Yellowknife District (Ramsay, 1973); mafic to felsic granulite grade gneisses from the Reading Prong,

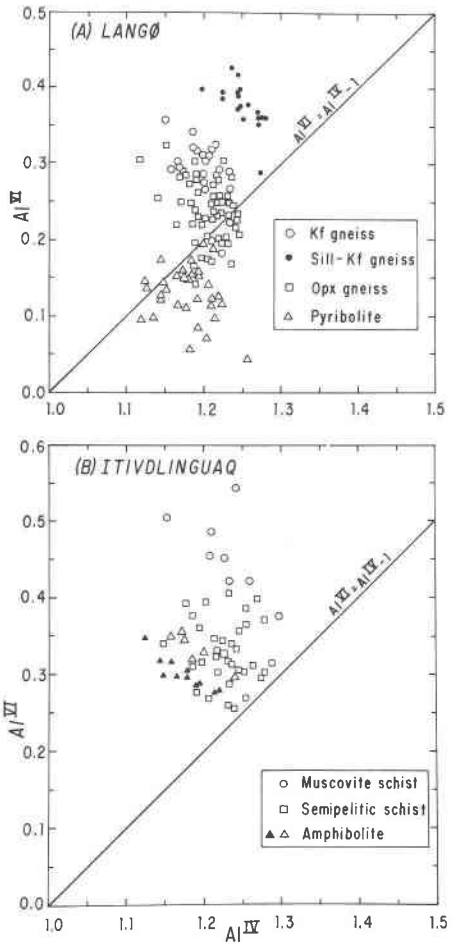

Fig. 4. Formula proportions of Al^{VI} and Al^{IV} in biotite from Langø (a) and Itivdlinguaq (b) based on the 7 cation normalization (A).

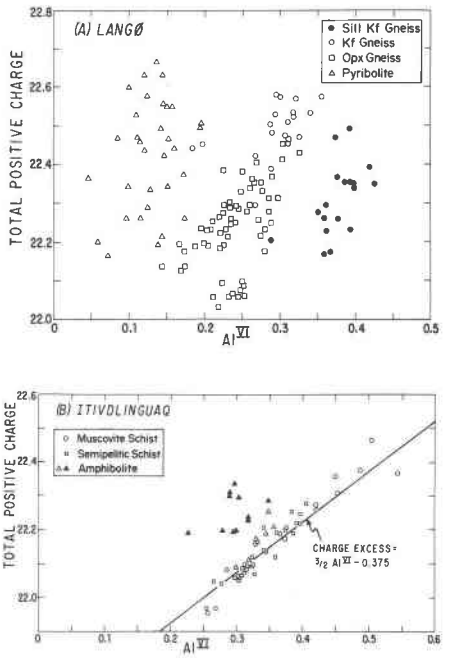

Fig. 5. Calculated total positive charge and Al^{VI}-content in biotite from Langø (a) and Itivdlinguaq (b), with formula proportions based on the 7 cation normalization.

New Jersey (Dallmeyer, 1974b); staurolite, staurolite–sillimanite and sillimanite–potassium feldspar zone metapelites, Maine (Guidotti *et al.*, 1975, 1977); cordierite–potassium feldspar and sillimanite–potassium feldspar zone metapelites, Bavaria (Blumel and Schreyer, 1977); and muscovite–sillimanite to sillimanite–potassium feldspar zone metapelites, Massachusetts (Tracy, 1978). These samples span a somewhat larger range of metamorphic grade than the ones from Greenland, and, except for the samples of Ramsay (1973) and Dallmeyer (1974b), represent predominantly Al-saturated biotite from limiting assemblages.

Ti-contents and calculated total positive charge for these data sets are illustrated in Figure 10, with formula proportions based on normalization (A). All analyses yield a charge excess that to a greater or lesser extent correlates with Ti-content (*cf.*, Fig. 2). Except for the data of Dallmeyer, calculated positive charge for all but one analysis falls above the Charge Excess = 2Ti lines.

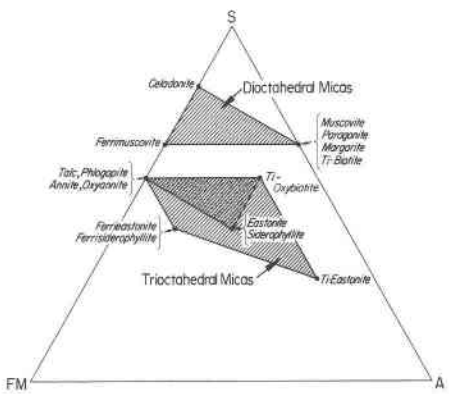

Fig. 6. Ternary representation of mica compositions, with coordinates defined as follows:

$$S = SiO_2 + 2K_2O + 2Na_2O + 2BaO + 2CaO$$

$$A = 2Al_2O_3 + 2Cr_2O_3 + 2TiO_2 - 2K_2O - 2Na_2O - 2BaO - 2CaO$$

$$FM = FeO_T + MgO + MnO + ZnO - TiO_2$$

All compositions prefixed by "ferri" have Fe^{3+} in lieu of Al^{3+} in octahedral sites. Ti-biotite is the Ti-vacancy end-member, siderophyllite is the ferrous iron analogue of eastonite, and celadonite is $K(AlMg\square)Si_4O_{10}(OH)_2$; other compositions are given in the text. The stippled region in the trioctahedral mica field is expanded in Fig. 7.

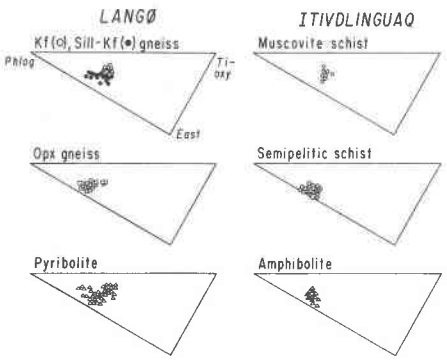

Fig. 7. Compositions of West Greenland biotites portrayed in S–A–Fm coordinates, as indicated in Fig. 6. The data points all lie within the region bounded by phlogopite–eastonite–Ti-oxybiotite; the fact that the data are shifted off the phlogopite–eastonite join towards the S corner indicates the presence of a Ti-oxycomponent, a Ti-vacancy component, or a muscovite component (*cf.*, Fig. 6)

Similarly, except for Dallmeyer's data, all analyses have $Al^{VI} > Al^{IV}$ as shown in Figure 11. Thus, for the relatively Al-poor analyses of granulite grade biotite, calculated charge excess is compensated almost com-

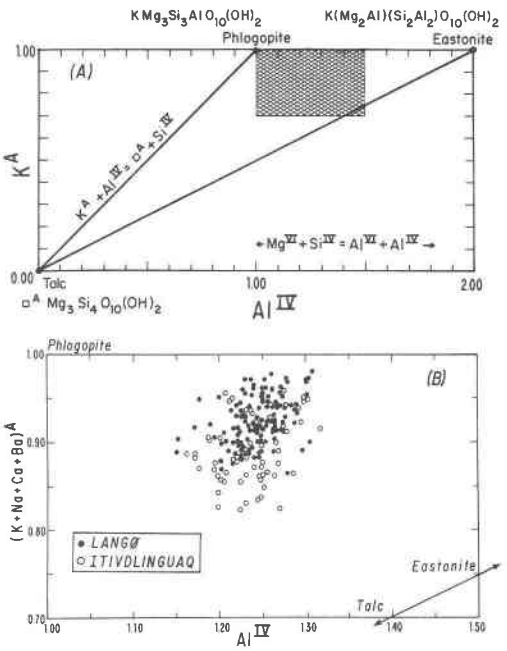

Fig. 8. (a) K^A–Al^{IV} variation diagram illustrating the substitutional relationships among talc, phlogopite, and eastonite. (b) Expansion of the stippled region shown in (a) illustrating A-site occupancy *vs.* Al^{IV} in the Greenland biotites, with formula proportions based on the 11 oxygen normalization (B). No systematic difference is apparent between the two data sets, although the analyses of biotite from Itivdlinguaq extend to lower A-site occupancy.

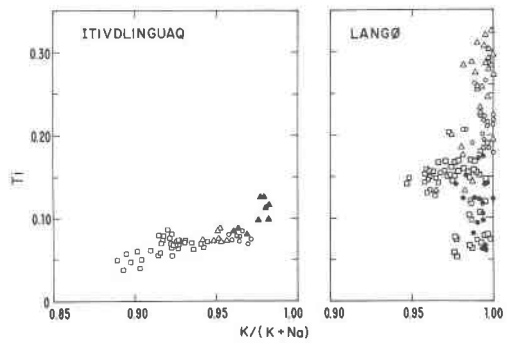

Fig. 9. Ti *vs.* K/(K+Na) in biotite from West Greenland; symbols as in previous figures.

pletely by Ti-substitution, whereas for the other data sets involving relatively Al-rich biotite, charge excess is compensated by both Ti and Al^{VI}. These relationships (Figs. 10 and 11) do not contradict any of the previously stated conclusions regarding Ti- and Al-substitution in the Greenland biotites, and appear to lend them strong support.

Ti-vacancy vs. Ti-oxy substitution

The correlations between Ti and calculated positive charge in biotite from West Greenland (Fig. 2) and elsewhere (Fig. 10) are ambiguous because they are consistent with two interpretations that are not necessarily mutually exclusive: vacancies and oxycomponents.

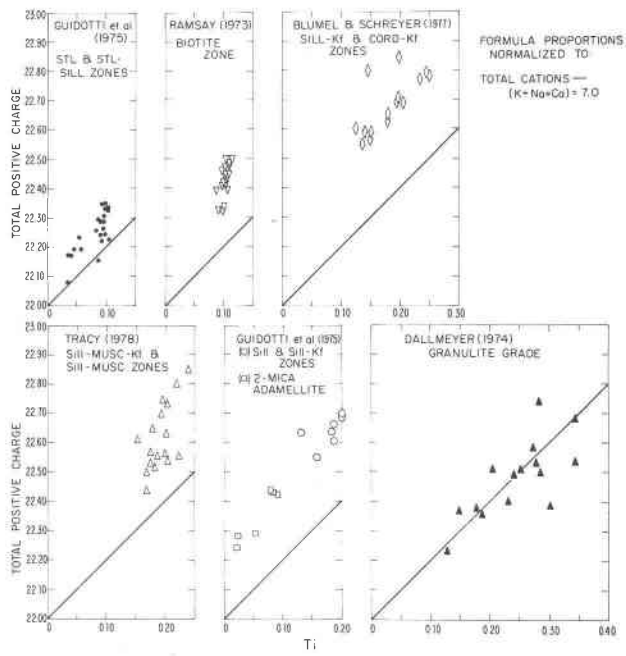

Fig. 10. Calculated total positive charge and Ti-contents in biotite from the various localities cited in the text, with formula proportions based on the 7 cation normalization (A).

The graphical treatment of mica compositions (Fig. 7) resulted in the same ambiguity.

The data presented in this report together with observations made previously by other workers strongly support the conclusion that the Ti-content of biotite coexisting with a Ti-oxide phase increases with grade of metamorphism, commonly reaching extreme values in granulite grade rocks (>6 wt.%). A consequence of this observation is that Ti increases the stability field of biotite.

It follows from this conclusion that either vacancy-formation or oxy-substitution promote an increased stability for biotite. The formation of vacancies in biotite may create a crystallographically favorable environment for increased Ti-substitution. An oxycomponent, on the other hand, might provide a partial explanation for the ubiquitous occurrence of a "hydrous" phase (*i.e.*, biotite) in otherwise "anhydrous" rocks such as granulites. Stated another way, Ti-substitution in biotite could involve progressive "dehydration."

Incorporation of Ti into biotite as an oxycomponent would result in a distinct negative correlation between Ti and $(OH)^-$, which is virtually impossible to test utilizing the microprobe analyses presented here. Nevertheless, assuming that the difference between the analytical total and 100% represents the H_2O-content, the calculated formula proportions of $(OH)^-$ were compared to Ti-content. Examination of the data revealed no correlation whatsoever, but this may not be a meaningful test, due to the large uncertainties involved.

Evaluation of analyses for which direct H_2O determinations are available provide an alternative approach to this problem. Stevens (1946) observed that many wet chemical analyses of mica minerals were deficient in $(OH)^-$, and was the first to suggest that this deficiency is compensated by a Ti-oxycomponent. Foster (1964) likewise noted that calculated $(OH)^-$ contents of many trioctohedral micas were less than the theoretical 2.0/formula, but also observed that O^{2-} contents showed a corresponding excess. She concluded that an oxyannite component (9) could accomodate some, but not all of this deficiency.

Dodge *et al.* (1969) pointed out that the $(OH)^-$ deficiencies discussed by Stevens (1946) might be due to incorrect analyses of water content. Consequently, they took particular care in carrying out H_2O-determinations in their study of biotite in granitic rocks from the Sierra Nevada batholith. Despite this, all but one of their analyses yielded $(OH+F+Cl) < 2.0$, and they also attributed this deficiency to an oxyannite component. An examination of their analyses by the writer reveals no correlation between Ti and $(OH)^-$.

Forbes (1972) also studied variation in the hydroxyl content of biotite, and showed that a remarkable correlation exists ($r^2 = -0.96$) between $\Sigma(OH+F+Cl)$ and the difference in charge calculated for cations in octahedral and tetrahedral sites [*i.e.*, $\Delta_{charge} = \Sigma\ VI_{charge} - \Sigma\ IV_{charge}$]. The correlation between hydroxyl content and interlayer site charge was very poor ($r^2 = -0.22$), indicating that <5% of the observed $(OH)^-$ variation could be ascribed to interlayer cations. In order to explain his observations, Forbes postulated the existence of "tetrasilicic phlogopite" [$KMg_3Si_4O_{11}(OH)$], which is related to phlogopite by the substitution: $Si^{4+} = Al^{3+} + H^+$. Although Forbes was able to synthesize this compound, he determined that it was unstable with respect to other phases; its role in the compositional variation of naturally occurring biotites is unclear.

Experimental studies lend support to both vacancy- and oxy-substitution. For example, Forbes and Flower (1974) synthesized a Ti-vacancy biotite in the Mg-system, whereas Abrecht and Hewitt (1980, 1981) produced biotites with various amounts of Ti-vacancy, Ti-oxy and Ti-Tschermak's substitutions. The latter authors were unable to find evidence for a vacancy substitution in the Fe-system.

Hazen and Burnham (1973) considered Ti-substitution in biotite and noted that the cation configuration $(R^{2+}Ti\square)^{VI}Si^{IV}$ yields an ideal +2 charge contribution to nearest oxygen atoms. These same authors also noted (p. 898) that their structural refinements of Pike's Peak annite indicated the presence of octahedral vacancies approximately equal in number to the amount of Ti.

Takeda and Ross (1975) reported a crystallographic study of oxybiotite in a rhyodacite ash flow tuff from the Valles Mountains, New Mexico, and concluded that subequal amounts of an oxyannite component and a Ti-oxycomponent are present in this sample. Bohlen *et al.* (1980) described a biotite in orthogneiss from the Au Sable Forks area, New York, and concluded that an oxycomponent represented the dominant mechanism for Ti-substitution in their sample.

Studies of the infrared spectra of micas have revealed several interesting features relevant to the present discussion. Such spectra are, in general, characterized by three sets of absorption bands termed N (normal), I (impurity) and V (vacancy) (Vedder, 1964). N- and I-bands are produced by stretching of (OH) oriented approximately normal to the mica *a–b* plane (Serratosa and Bradley, 1958). Three separable N-bands may occur, which show a frequency shift in response to $Mg–Fe^{2+}$ variation; these have been ascribed to cation-hydroxyl configurations such as Mg_3^{2+}–(OH), $Mg_2^{2+}Fe^{2+}$–(OH), and $Mg^{2+}Fe_2^{2+}$–(OH) (Wilkins, 1967). I-bands are associated with various $R^{2+}R^{3+}$–(OH) configurations (Wilkins, 1967), and their frequencies and intensities have been correlated to variations in the abundance of $(Al, Fe^{3+})^{VI}$ (Rousseaux *et al.*, 1973).

V-bands display pronounced infrared dichroism, and are related to stretching of (OH) which lies approximately within the mica *a–b* plane and is coordinated to two cations and a vacancy. Thus V-bands in biotite are not unlike absorption bands associated with the vacant site in dioctohedral micas, such as muscovite (Vedder and McDonald, 1963; Vedder, 1964).

Three overlapping, but resolvable V-bands are com-

monly observed, the intensities of which vary as a function of mica composition (Vedder, 1964) and water content (Rouxchet, 1970). However, the cation configurations that yield V-bands are somewhat uncertain. Vedder (1964) initially suggested R^{2+}–R^{2+}–□(OH), R^{2+}–R^{3+}–□(OH) and R^{3+}–R^{3+}–□(OH). Farmer *et al.* (1971) noted that the intensity of two of the V-bands is greatest in biotite with high Al and Fe^{3+}, and made specific assignments for Fe^{2+}–Fe^{3+}–□(OH) and Fe^{2+}–Al^{3+}–□(OH). Neither Vedder (1964) nor Farmer *et al.* (1971) considered the explicit involvement of Ti in any of the observed spectra. However, Rousseaux *et al.* (1973) noted that Mg-rich biotite with low contents of Al and Fe^{+} displayed a single strong V-band which they assigned to R^{2+}–Ti^{4+}–□(OH). They extended this assignment to other biotites based on the characteristic frequency of this absorption band. The important point here is the spectroscopic identification of (OH) absorption bands associated with octahedral vacancies in biotites with a wide range of chemical compositions.

Vedder and Wilkins (1969) carried out a series of dehydroxylation studies on several micas, and noted that the V-bands disappeared from the biotite spectra at temperatures in the range 500–800°C, whereas N- and I-bands persisted to at least 900°C. They suggested that in biotite, as in muscovite, two $(OH)^-$ near an octahedral vacancy condensed to form H_2O, which then leaves the mica by diffusion. In the case of biotite, $(OH)^-$ near a vacancy is expelled long before those associated with a completely filled octahedral site (Vedder and Wilkins, 1969).

These authors also noted that *in situ* oxidation of Fe^{2+} to Fe^{3+}, with concomitant loss of H_2 [oxyannite (9)] might complicate this interpretation. However, the fact that V-band intensity could not be restored by hydrogenation confirmed that hydroxyl loss occurred by H_2O condensation, and not by simple hydrogen loss. In contrast, the intensities of N- and I-bands can be nearly completely restored by hydrogenation, indicating that no large loss of (OH) by condensation from N or I "sites" has occurred, but rather by hydrogen loss associated with oxidation of Fe^{2+}.

In summary, observations on variations of the H_2O-content in biotite do not offer a solution to the problem of Ti-vacancy *vs.* Ti-oxy substitution, and most investigators would seem to favor an oxyannite component as the principal source of this variation. The results of X-ray crystallographic and experimental studies do not establish a unique mechanism for Ti-substitution either (and it may turn out ultimately that more than a single one is involved). The results of infrared spectral studies support the vacancy substitution, whereas the dehydroxylation experiments may provide a possible explanation for some evidence favoring the Ti-oxycomponent: Ti initially enters biotite via a vacancy substitution, and later (in response to some thermal event?), H_2O is lost by $(OH)^-$ condensation producing an oxygen "excess." This mechanism could also explain the low water contents in some biotite analyses.

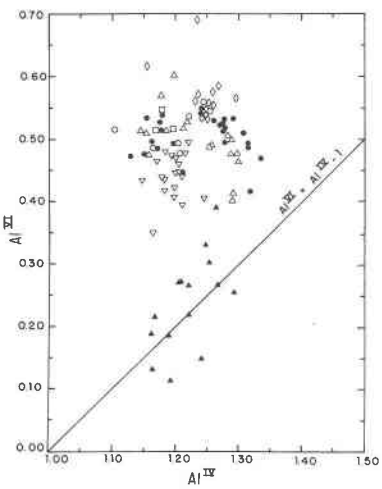

Fig. 11. Formula proportions of Al^{VI} and Al^{IV} in biotite from the various localities cited in the text, with formula proportions based on the 7 cation normalization (A); symbols as in Fig. 10.

Collectively, the observations outlined above do not contraindicate a Ti-vacancy substitution, and the writer tentatively concludes that it provides the best explanation for Ti-substitution in the biotites considered here. The remaining sections of this paper explore some consequences of this interpretation.

An iterative normalization

If Ti-substitution in biotite involves vacancies, as suggested here, then the 7 cation normalization procedure (A) is incorrect and should be abandoned. A more appropriate cation-based normalization scheme would be:

$$\text{Total Cations} - (K+Na+Ca+Ba) + Ti = 7.0, \quad \text{(C)}$$

which allocates a vacancy for each Ti cation. However, normalization (C) does not eliminate charge excess in many analyses, particularly in those with large amounts of Al^{VI}.

Therefore, a fourth normalization procedure can be carried out, which takes into account vacancies associated with Al-substitution by means of the dioctahedral component [substitution (2)]. The Al of interest in (2) is actually excess octahedral $R^{3+}(=Al^{VI}_{xc})$, where:

$$Al^{VI}_{xc} = (Al+Cr)^{VI} - Al^{IV} + (K+Na+2Ca+2Ba) \qquad (11)$$

so that the fourth normalization takes the following form:

$$\text{Total Cations} - (K+Na+Ca+Ba) + Ti + \tfrac{1}{2}Al^{VI}_{xc} = 7.0, \quad \text{(D)}$$

which allocates one vacancy for every two excess octahedral Al ions in addition to the vacancy already allocated to Ti. Normalization of analyses according to (D) eliminates calculated charge excess in all cases and permits a

Table 7. Selected examples of biotite formula proportions calculated on the basis of the iterative normalization procedure.

		1.	2.	3.	4.	5.	6.	7.	8.	9.
IV	Si	2.727	2.724	2.727	2.800	2.680	2.690	2.790	2.773	2.756
	Al	1.273	1.276	1.273	1.200	1.289	1.310	1.210	1.227	1.244
	Fe3+	0.000	0.000	0.000	0.000	0.031	0.000	0.000	0.000	0.000
VI	Al	0.316	0.191	0.114	0.093	0.000	0.437	0.333	0.283	0.209
	Fe3+	0.042	0.142	0.257	0.167	0.416	0.100	0.012	0.066	0.103
	Ti	0.123	0.206	0.143	0.134	0.292	0.075	0.069	0.073	0.127
	Mg	1.765	1.217	1.921	2.193	1.453	1.273	1.640	1.638	1.282
	Fe2+	0.625	1.021	0.421	0.276	0.537	0.929	0.876	0.865	1.145
	Mn	0.006	0.011	0.002	0.002	0.002	0.021	0.000	0.000	0.008
	Zn	0.000	0.006	0.001	0.000	0.007	0.001	0.003	0.001	0.000
	Σ	2.877	2.794	2.857	2.866	2.707	2.837	2.931	2.927	2.873
A	Ca	0.002	0.000	0.001	0.000	0.000	0.000	0.000	0.000	0.000
	Na	0.010	0.000	0.031	0.035	0.003	0.027	0.068	0.051	0.019
	K	0.901	0.944	0.871	0.905	0.901	0.920	0.798	0.826	0.913
	Σ	0.913	0.944	0.902	0.940	0.904	0.947	0.866	0.877	0.932
Charge*		21.958	21.858	21.743	21.833	21.553	21.900	21.988	21.934	21.897

1. Table 1, #1 (OGA-24c Sill-Kf gneiss) 2. Table 1, #5 (OGA-27 Kf gneiss) 3. Table 2 #4 (OGA-28h Opx gneiss) 4. Table 3, #1 (OGA-23b Pyribolite) 5. Table 3, #6 (OGA-36k Pyribolite) 6. Table 4, #2 (OGA-48g Muscovite schist) 7. Table 5, #6 (OGA-48r-2 Semipelitic schist) 8. Table 6, #1 (OGA-48ab Amphibolite) 9. Table 6, #6 (OGA-48a Hornblende amphibolite)

* *Total positive charge calculated with all iron as* Fe^{2+}

rough estimate for Fe^{3+} [excluding that associated with oxyannite (9)].

It turns out that normalization (D) works only for Al-rich biotite, as most Al-poor analyses yield negative Al^{VI}_{xc}. This effect most probably reflects the presence of octahedral Fe^{3+}, the amount of which is not known prior to normalization. Nevertheless, the "negative magnitude" of Al^{VI}_{xc} provides a minimum estimate of Fe^{3+} needed to balance Al^{IV}. Formula proportions for a selected number of analyses from Tables 1–6 calculated from the iterative normalization are listed in Table 7.

Model system for mica composition

The substitutional relationships discussed previously for Ti and Al (excepting oxycomponents) are summarized in a hypothetical mica composition polyhedron illustrated in Figure 12. Although this diagram was constructed for the Mg–Al system, Fe^{2+} and Fe^{3+} components can be substituted at each composition point where appropriate.

Figure 12 distinguishes those cation substitutions [(1), (2), (3), (6)] that are accessible directly from phlogopite from those Ti-substitutions [(4), (5)] which require an aluminous component as well. Stated another way, [(2)–(5)–(6)] and [(1)–(3)–(4)] are respective linear combinations of each other. Some of the substitutions shown in Figure 12 are in fact redundant, and it can be shown that many proposed substitutions in micas are linear combinations of an Al-Tschermak's component (1), a dioctohedral component (2), a Ti-spinel component (5), and a talc component (10), coupled with the simple cation exchange components Fe = Mg, K = Na, Al = Fe^{3+} and Al = Cr. A plagioclase component (NaSi = CaAl) and a simple Ba = Ca exchange would relate all brittle micas to the system shown in Figure 12.

For example, the Ti-Tschermak's (3) and TiAl = AlSi (4) substitutions are linear combinations of the Al-Tschermak's (1) and Ti-spinel (5) components [(3) = (5)–2(1) and (4) = (5)–(1)]. Robert (1976b) suggested that the following substitution represents an independent method for producing octahedral vacancies:[7]

$$2Al^{IV} + Mg^{VI} = 2Si^{IV} + \square^{VI}. \qquad (12)$$

Substitution (12) is, in fact, a linear combination of the Al-Tschermak's (1) and dioctohedral (2) components [(12) = (2)–2(1)].

Holdaway (1980) considered chemical formulae appropriate for "averge" biotite compositions in medium- to high-grade pelitic schists, and was particularly concerned about how to deal with $(Ti, Al)^{VI}$. Although he noted (p. 714) that ". . . octahedral sites for Ti-free biotite are 98% full and octahedral vacancies increase with Ti . . .", he remarked that the Ti-vacancy substitution (6) was probably not a good assumption. By carrying out a linear least squares regression on 47 microprobe analyses of biotite [including the data of Guidotti *et al.* (1977) and Tracy (1978), which have also been considered here (*cf.*, Figure 10)], he deduced the following complex substitutional relationship:

$$(R^{2+})^{VI}_{1.25} + (Al^{3+})^{VI}_{0.67} + \square^{A}_{0.50} = (Ti^{4+})^{VI}_{1.00} + \square^{VI}_{0.92} + K^{A}_{0.50}. \qquad (13)$$

However, he considered (13) to represent the sum of two grade-dependent substitutions:

[7] In this study, Robert also described the systematic increase in the intensity of the infrared V-band.

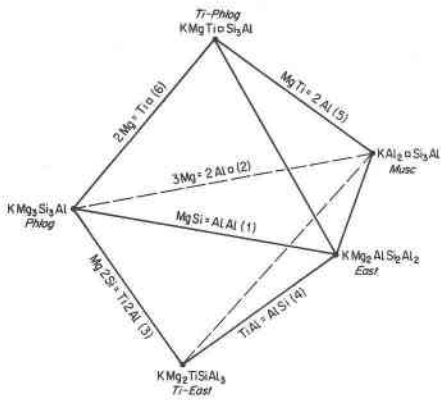

Fig. 12. Hypothetical mica composition polyhedron derived from the substitutional components described in the text. In general, many substitutions in micas can be shown to be linear combinations of (1), (2) and (5), so that even in this simple representation, some of the substitutions are redundant.

$$(R^{2+})^{VI}_{1.00} + (Al^{3+})^{VI}_{0.67} = (Ti^{4+})^{VI}_{1.00} + \square^{VI}_{0.67} \quad (14a)$$

$$(R^{2+})^{VI}_{0.25} + \square^{A}_{0.50} = \square^{VI}_{0.25} + K^{A}_{0.50}. \quad (14b)$$

In terms of the substitutions considered here, (13) and (14) represent linear combinations of Al-Tschermak (1), dioctohedral (2), Ti-vacancy (6), and talc (10) components [(14a) = (6) − 0.33(2) and (14b) = 0.25(2) − 0.5(1) − 0.5(10), such that (13) = (6) − 0.5(1) − 0.083(2) − 0.5(10)]. The additivity of the substitutions leading to (13) serves to illustrate why $Ti^{VI} \simeq \square^{VI}$.

It was suggested to the writer in review that substitutions other than a talc component (10) may cause variations in the occupancy of the interlayer site. Two of these could be:

$$K^{A} + (R^{2+})^{VI} = \square^{A} + (R^{3+})^{VI}, \text{ and} \quad (15)$$

$$K^{A} + (R^{3+})^{VI} = \square^{A} + (Ti^{4+})^{VI}. \quad (16)$$

However, (15) and (16) are also linear combinations of the principal substitutions discussed here [(15) = (1) + (10) and (16) = (2)–(10)–(6)–(1)].

The model system has an interesting consequence for Ti substitution in micas. Specifically, the Ti-vacancy substitution (6) is actually a linear combination of the dioctohedral (2) and Ti-spinel (5) components [(6) = (2)–(5)]. Thus Ti-substitution in muscovite occurs directly by (5) whereas in biotite it is by a combination of (5) and (2). This interpretation helps to explain why the correlation between Ti-content and calculated positive charge is best in biotite with low Al^{VI}.

Using this model system, together with formula proportions derived from the iterative normalization method (D), and Fe^{3+} estimated from charge calculations, it is possible to cast any biotite analysis into end-members. End-members calculated from the analyses listed in Table 7 are presented in Table 8.

Crystal–chemical considerations

It has been known for some time that the lateral dimensions of the octahedral and tetrahedral sheets in biotite do not match precisely. Donnay *et al.* (1964) indicated that this structural misfit between the sheets is accommodated primarily by a rotation of the tetrahedra about [001] (see Fig. 1 of McCauley and Newnham, 1971), and in phlogopite the tetrahedral rotation angle (α) is approximately 8°. Hazen and Wones (1972) have discussed how substitution of Fe^{2+} (0.78Å) for Mg^{2+} (0.72Å) causes the octahedral sheet to expand, which increases

Table 8. Mica end-members calculated for analyses listed in Table 7.

	End-Member	Formula*	1.	2.	3.	4.	5.	6.	7.	8.	9.
(A)	Talc	$(\square)^{A}(Mg_3)^{VI}(Si_4)^{IV}O_{10}(OH)_2$	8.7	5.6	9.7	6.0	9.6	5.3	13.4	12.3	6.8
(B)	Ti-Phlogopite	$(K)^{A}(MgTi\square)^{VI}(Si_3Al)^{IV}O_{10}(OH)_2$	12.3	20.6	14.3	13.4	29.2	7.5	6.9	7.3	12.7
(C)	Ferri-Eastonite	$(K)^{A}(Mg_2Fe^{3+})^{VI}(Si_2Al_2)^{IV}O_{10}(OH)_2$	4.2	14.2	25.7	16.7	41.6	10.0	1.2	6.6	10.3
(D)	Muscovite	$(K)^{A}(Al_2\square)^{VI}(Si_3Al)^{IV}O_{10}(OH)_2$	0.0	0.0	0.0	0.0	0.0	8.8	0.0	0.0	0.0
(E)	Eastonite	$(K)^{A}(Mg_2Al)^{VI}(Si_2Al_2)^{IV}O_{10}(OH)_2$	31.6	19.1	11.2	9.3	0.0	26.3	33.2	28.3	20.9
(F)	Phlogopite	$(K)^{A}(Mg_3)^{VI}(Si_3Al)^{IV}O_{10}(OH)_2$	43.2	40.	39.1	54.5	19.6	42.1	45.3	45.5	49.3
		$Mg/(Mg+Fe_T)$	.726	.511	.739	.832	.596	.553	.649	.638	.507
		$Mg/(Mg+Fe^{2+})$	.738	.544	.820	.888	.730	.578	.652	.654	.528
		Fe^{2+}/Fe_T	.937	.878	.621	.623	.546	.903	.986	.928	.917

(A) = 1.0 - (K+Na+Ca+Ba); (B) = Ti; (C) = $(Fe^{3+})^{VI}_{calc}$; (D) = 0.5 X [$(Al+Cr+Fe^{3+})^{VI}$ - $(Al^{IV}$-K-Na-2Ca-2Ba)];

(E) = $(Al+Cr)^{VI}$ - 2 X D; (F) = 0.333 X [R^{2+} - 3 X A - 2 X (C+E) - B]

* *Na, Ca, Ba grouped with K; Fe^{2+}, Mn, Zn grouped with Mg.*

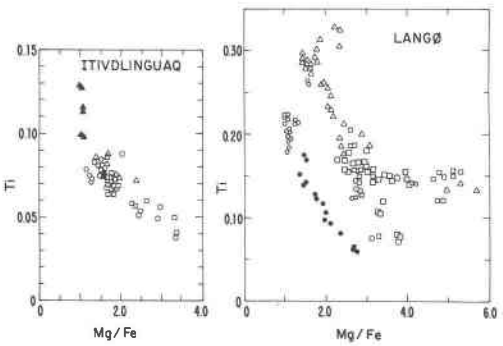

Fig. 13. Ti-content *vs.* Mg/Fe in biotite from West Greenland, with formula proportions based on the iterative cation normalization (D); symbols as in previous figures.

both the structural misfit and α. Fe-substitution reaches a limit where the mean octahedral radius is ~0.76Å, which corresponds to Fe/(Fe + Mg) ~ 0.67. At this point, α = 0°, and the tetrahedra constitute a regular hexagonal array. Compositions with more iron are stable only if there is oxyannite substitution, *i.e.*, the presence of Fe^{3+} decreases the dimension of the octrahedral sheet and promotes additional Fe^{2+} substitution.

Similarly, substitution of the smaller Ti^{4+} cation (0.605Å) should promote increased Fe/Mg, or more probably, high Fe/Mg favors increased Ti-substitution. Figure 13 shows that in the Greenland biotites, Ti tends to decrease with increaing Mg/Fe, although there appear to be two distinct trends in the Langø data, which are probably related to differences in Al-content. Since most of the biotite analyses presented here are Ti-saturated, the relationships shown in Figure 13 are consistent with some type of crystal–chemical control on Ti-substitution by Fe/Mg. Thus the structural distortions caused by increased Fe/Mg are partly offset by increasing Ti. In addition, the presence of octahedral vacancies associated with Ti should permit the necessary structural accommodations to occur more easily. However, the effects of Ti on the structure of biotite must be considered in view of the fact that the tetrahedral sheet is not Si_3Al as in phlogopite-annite, but distinctly more aluminous (*cf.*, Figs. 2 and 4).

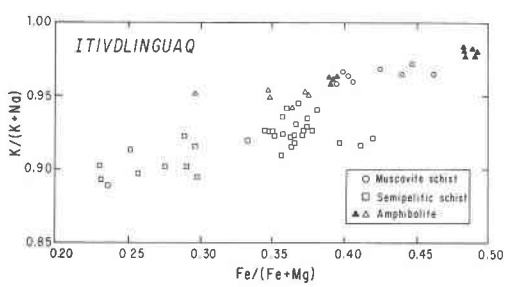

Fig. 14. K/(K+Na) *vs.* Fe/(Fe+Mg) in amphibolite grade biotite from Itivdlinguaq, which shows that the most Mg-rich biotites are also the most Na-rich.

Substitution of either the Al- or Ferri-Tschermak's components causes expansion of the tetrahedral sheet and contraction of the octahedral sheet, with a resulting increase in structural misfit. Although tetrahedral rotation occurs to compensate for this added misfit, the rotation is limited by the minimum bond length associated with the interlayer cation, *i.e.*, tetrahedral rotation cannot proceed beyond the point where the mean K–O bond length decreases to 2.8Å (Hewitt and Wones, 1975). These authors indicated that this limit to the rotation angle would then limit Al-substitution in K-biotite, but they were able to synthesize a more aluminous biotite in the Na system, in which case the smaller interlayer cation permits a greater amount of tetrahedral rotation to occur.

The amount of Tschermak's components in the Greenland biotites, as gauged by Al^{IV} (Figs. 2 and 4), is similar in analyses from both the amphibolite and granulite grade localities. However, the biotite from Itiv contains more Al^{VI} than that from Langø (Fig. 4), and the decrease in the size of the octahedral sheet associated with this extra Al^{VI} would necessitate additional tetrahedral rotation. The fact that the more aluminous biotite from Itiv is also more sodic (Fig. 9) suggests that the required extra tetrahedral rotation is compensated by increased Na-substitution. In the granulite grade biotite from Langø, which contains abundant Ti that should also increase structural misfit, it may be unnecessary to incorporate the smaller Na cation since contraction of the octahedra in this case is not as great where the larger Ti is dominant over the smaller Al.

However, Fe/Mg in biotite may exert a more fundamental control on K/Na. In samples from Langø, the most Mg-rich biotite contains the highest amount of Na, and in the analyses from Itiv, K/(K + Na) increases uniformly with increasing Fe/(Fe + Mg) (Fig. 14). Therefore, the expansion of the octahedral sheet and corresponding decrease in α caused by substitution of Fe for Mg, which is reversed by Ti (and Al) substitution, is counterbalanced slightly by a higher K-content in more Fe-rich biotite, since increasing K/(K + Na) also causes α to decrease.

Two representations of Ti and Al^{VI} in the Greenland biotites are illustrated in Figure 15. In both diagrams, there is a broad general decrease of Ti with increasing Al^{VI}. However, the positions of individual data points in Figure 15b, which is based on the iterative cation normalization procedure (D), are systematically shifted towards lower values of Al^{VI} compared to Figure 15a, which is based on the 7 cation normalization (A). Data points for the 11 oxygen normalization (B) plot at intermediate positions.

The shift in Figure 15 occurs because the abundance of each cation is lowered using the iterative normalization: Si decreases, which increases Al^{IV}, and Al^{VI} decreases as a result. Therefore, the difference between Figures 15a and 15b is to some extent an "artifact" of the normalization process. Note however that analyses of Ti-rich

biotite yield little to no Al^{VI} in Figure 15b. In several of these analyses, (Si + Al) is less than 4.0, and, in general, the higher the Ti-content, the lower the sum of Al + Si. The data indicate up to 0.15 cations of an additional element in tetrahedral coordination, and the most logical candidate is Fe^{3+}. Czamanske and Wones (1973) have also noted the possible occurrence of tetrahedral Fe^{3+} in biotite with high contents of Ti. Although high Ti in biotite may be partly accommodated by $(Fe^{3+})^{IV}$, since it would tend to decrease structural misfit, this assignment is problematic due to the lack of reverse pleochroism in these samples (*cf.*, Farmer and Boettcher, 1981).

Summary and conclusions

This report has summarized in detail the principal characteristics of biotite in a range of rock types from two localities in West Greenland. Compared to amphibolite grade biotite, those in granulite grade samples are characterized by higher Ti, similar Al^{IV}, and lower Al^{VI}; K/(K + Na) and possibly Σ(K + Na) are also higher in granulite grade biotite. Chemical variation at each locality is strongly dependent on rock composition and mineral assemblage.

Substitution of Ti, and to a lesser extent Al, on octahedral sites in biotite is interpreted in terms of vacancy-formation. Based on these conclusions, an iterative cation-based normalization procedure is described that eliminates charge excess associated with Ti and Al, and permits Fe^{3+} to be estimated from the relationship: Fe^{3+} = 22.0 − Total Positive Charge. Fe^{3+} calculated by this method ranges from 0.05–0.45 Fe_T, with the largest amounts occurring in biotite from pyribolites, which are magnetite-bearing, and the smallest amounts in muscovite schists and sill-Kf gneisses, some of which are graphite-bearing. In addition, formula proportions calculated from the iterative normalization for biotites with high TiO_2 (>5 wt.%), may indicate the occurrence of $(Fe^{3+})^{IV}$.

A mica composition polyhedron is presented which shows how complex substitutional mechanisms can be reduced to combinations of a few simple types, and that Ti-substitution in muscovite and biotite lead to the same end-member composition. Mica end-members were constructed utilizing these simple substitutions, and calculated Fe^{3+}.

The formulation of biotite analyses into end-members, as well as the methods for estimating Fe^{3+}, assume an anion framework with a net charge of −22.00 and no oxycomponents, although oxyannite substitution should not affect any of the conclusions reached here. Additional work on Ti-rich biotite, which combines high-quality hydrogen analyses with spectroscopic studies (infrared, optical, Mössbauer), together with X-ray crystallographic studies on site populations, is needed to explore further the interrelationships among Ti-content, vacancies and oxycomponents, and to evaluate the possible occurrence of tetrahedral Fe^{3+}.

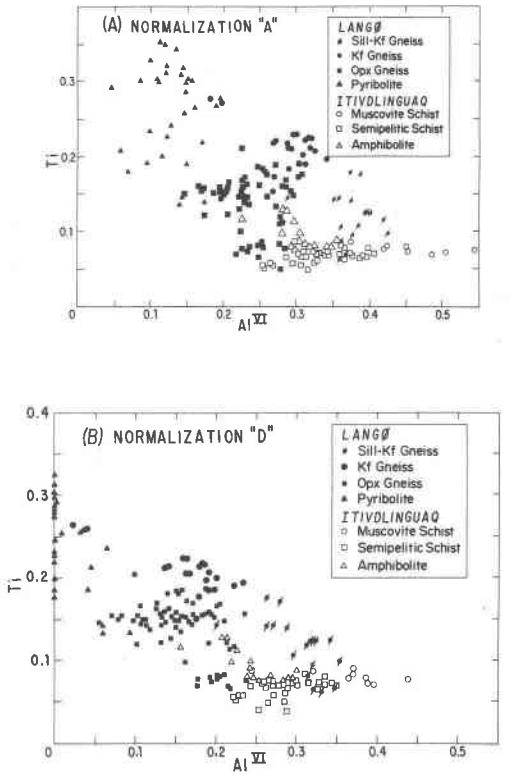

Fig. 15. Ti *vs.* Al^{VI} in biotite from West Greenland. In (a) formula proportions are based on the 7 cation normalization (A), and in (b) on the iterative cation normalization (D); note the systematic shift towards lower Al^{VI} when the iterative normalization is used.

Acknowledgments

The initial study of biotite in the Langø gneisses comprised part of a Ph.D. dissertation at the California Institute of Technology carried out under the supervision of A. L. Albee, with the financial support of NSF grant DES 75-03417. Completion of the manuscript was aided by the Clark Fund of Harvard University, and NSF grants EAR 78-23412 and EAR 81-09466. Support for additional field work in Greenland was provided by a grant from the National Geographic Society.

The writer wishes to thank J. B. Thompson for discussions on cation substitutions, and for suggesting the format of Figure 6. S. Dobos and C. A. Francis read an early version of the manuscript; thorough reviews by S. W. Bailey, D. A. Hewitt and D. R. Wones resulted in clarification of several issues, and are most appreciated. The writer also thanks V. R. McGregor, Geological Survey of Greenland, for providing some of the samples used in this study (prefixed GGU).

References

Abrecht, J. and Hewitt, D. A. (1980) Ti-substitution in synthetic Fe-biotites. (abstr.) Geological Society of America Abstracts with Programs, 12, 377.

Abrecht, J. and Hewitt, D. A. (1981) Substitutions in synthetic Ti-biotites. (abstr.) Geological Society of America Abstracts with Programs, 13, 393.

Albee, A. L. and Ray, L. (1970) Correction factors for electron

probe microanalysis of silicates, oxides, carbonates, phosphates, and sulfates. Analytical Chemistry, 42, 1408–1414.

Bence, A. E. and Albee, A. L. (1968) Empirical correction factors for the electron microanalysis of silicates and oxides. Journal of Geology, 76, 382–403.

Blumel, P. and Schreyer, W. E. (1977) Phase relations in pelitic and psammitic gneisses of the sillimanite–potash feldspar and cordierite–potash feldspar zones in the Moldanubicum of the Lam-Bodenmais Area, Bavaria. Journal of Petrology, 18, 431–459.

Bohlen, S. R., Peacor, D. R., and Essene, E. J. (1980) Crystal chemistry of a metamorphic biotite and its significance in water barometry. American Mineralogist, 65, 55–62.

Burns, R. G. and Vaughan, D. J. (1975) Polarized electronic spectra. In C. Karr, Ed., Infrared and Raman Spectroscopy of Lunar and Terrestrial Minerals, p. 39–72. Academic Press, New York.

Carman, J. H. (1974) Synthetic sodium phlogopite and its two hydrates: stabilities, properties, and mineralogic implications. American Mineralogist, 59, 261–273.

Champion, D. E., Albee, A. L., and Chodos, A. A. (1975) Reproducibility and operator bias in a computer controlled system for quantitative electron microprobe analysis. Proceedings of the 10th National Conference on Electron Probe Analysis, Las Vegas, 55.

Czamanske, G. K. and Wones, D. R. (1973) Oxidation during magmatic differentiation, Finnmarka Complex, Oslo Area, Norway: Part 2, The Mafic Silicates. Journal of Petrology, 14, 349–380.

Dahl, O. (1969) Irregular distribution of iron and magnesium among coexisting biotite and garnet. Lithos, 2, 311–322.

Dallmeyer, R. D. (1974a) The role of crystal structure in controlling the partitioning of Mg and Fe between coexisting garnet and biotite. American Mineralogist, 59, 201–203.

Dallmeyer, R. D. (1974b) Metamorphic history of the northeastern Reading Prong, New York and northern New Jersey. Journal of Petrology, 15, 325–360.

Dawson, J. B. and Smith, J. V. (1977) The MARID (mica-amphibole–rutile–ilmenite–diopside) suite of zenoliths in kimberlite. Geochimica et Cosmochimica Acta, 41, 309–323.

Delaney, J. S., Smith, J. V., Carswell, D. A., and Dawson, J. B. (1980) Chemistry of micas from kimberlites and zenoliths-II. Primary- and secondary-textured micas from peridotite zenoliths. Geochimca et Cosmochimica Acta, 44, 857–872.

Dodge, F. C. W. , Smith, V. C., and Mays, R. E. (1969) Biotites from granitic rocks of the central Sierra Nevada Batholith, California. Journal of Petrology, 10, 250–271.

Donnay, G., Donnay, J. D. H., and Takeda, H. (1964) Trioctohedral one-layer micas. II. Prediction of the structure from composition and cell dimensions. Acta Crystallographica, 17, 1374–1381.

Dymek, R. F. (1978) Metamorphism of the Archaean Malene Supracrustals, Godthåb District, West Greenland. In Proceedings of the 1978 Archaean Geochemistry Field Conference, p. 339–342. University of Toronto Press, Toronto, Canada.

Dymek, R. F. and Albee, A. L. (1977) Titanium and aluminum in biotite from high-grade Archaean gneisses, Langø, West Greenland. Transactions, American Geophysical Union (EOS), 58, 525.

Engel, A. E. J. and Engel, C. (1960) Progressive metamorphism and granitization of the major paragneiss, northwest Adirondack Mountains, New York, Pt. 2, Mineralogy, Geological Society of America Bulletin, 71, 1–58.

Eugster, H. P. and Wones, D. R. (1962) Stability relations of the ferruginous biotite, annite. Journal of Petrology, 3, 82–125.

Evans, S. and Raftery, E. (1980) X-ray photoelectron studies of titanium in biotite and phlogopite. Clay Minerals, 15, 209–218.

Farmer, G. L. and Boettcher, A. L. (1981) Petrologic and crystal-chemical significance of some deep-seated phlogopites. American Mineralogist, 66, 1154–1163.

Farmer, V. C., Russel, J. D., McHardy, W. J., Newman, A. C. D., Ahlrichs, J. L., and Rimsaite, J. Y. (1971) Evidence for loss of protons and octahedral iron from oxidized biotites and vermiculites. Mineralogical Magazine, 38, 121–137.

Faye, G. H. (1968) The optical absorption spectra of iron in six-coordinate sites in chlorite, biotite, phlogopite and vivianite. Some aspects of pleochroism in the sheet silicates. Canadian Mineralogist, 9, 403–425.

Faye, G. H. and Hogarth, D. D. (1969) On the origin of reverse pleochroism of a phlogopite. Canadian Mineralogist, 10, 25–34.

Forbes, W. C. (1972) An interpretation of the hydroxyl contents of biotites and muscovites. Mineralogical Magazine, 38, 712–720.

Forbes, W. C. and Flower, M. F. J. (1974) Phase relations of titan-phlogopite, $K_2Mg_4TiAl_2Si_6O_{20}(OH)_4$: A refractory phase in the upper mantle? Earth and Planetary Science Letters, 22, 60–66.

Foster, M. D. (1960a) Layer charge relations in the dioctahedral and trioctahedral micas. American Mineralogist, 45, 383–398.

Foster, M. D. (1960b) Interpretation of the compositions of trioctahedral micas. U.S. Geological Survey Professional Paper 354-B, 11–48.

Foster, M. D. (1964) Water content of micas and chlorites. U.S. Geological Survey Professional Paper 474-F.

Goldman, D. and Albee, A. L. (1977) Correlation of Mg/Fe partitioning between garnet and biotite with $^{18}O/^{16}O$ partitioning between quartz and magnetite. American Journal of Science, 277, 750–767.

Guidotti, C. V., Cheney, J. T., and Conatore, P. D. (1975) Interrelationship betwen Mg/Fe and octahedral Al content in biotite. American Mineralogist, 60, 849–853.

Guidotti, C. V., Cheney, J. T., and Guggenheim, S. (1977) Distribution of titanium between coexisting muscovite and biotite in pelitic schists from northwestern Maine. American Mineralogist, 62, 438–448.

Hazen, R. M. and Burnham, C. W. (1973) The crystal structure of one-layer phlogopite and annite. American Mineralgoist, 58, 889–900.

Hazen, R. M. and Wones, D. R. (1972) The effect of cation substitutions on the physical properties of trioctohedral micas. American Mineralogist, 57, 103–129.

Hewitt, D. A. and Wones, D. R. (1975) Physical properties of some synthetic Fe–Mg–Al trioctohedral biotites. American Mineralogist, 60, 854–862.

Holdaway, M. J. (1980) Chemical formulae and activity models for biotite, muscovite, and chlorite applicable to pelitic metamorphic rocks. American Mineralogist, 65, 711–719.

Holdaway, M. J. and Lee, S. M. (1977) Fe-Mg cordierite stability in high-grade pelitic rocks based on experimental, theoretical and natural observations. Contributions to Mineralogy and Petrology, 63, 175–198.

Keusen, H. R. and Peters, Tj. (1980) Preiswerkite, an Al-rich trioctohedral sodium mica from the Geisspfad ultramafic complex (Penninic Alp). American Mineralogist, 65, 1134–1137.

Kunitz, W. (1936) Beitrag zur kenntis der magmastischen Asso-

ziationex. III. Die Rolle des Titans und Zirkoniums in den gesteinbildenden Silikaten. Neues Jahrbuch für Mineralogie, Geologie und Paläontologie, 70, 385–416.

Kwak, T. A. P. (1968) Ti in biotite and muscovite as an indication of metamorphic grade in almandine amphibolite facies rocks from Sudbury, Ontario. Geochimica et Cosmochimica Acta, 32, 1222–1229.

Ludington, S. and Munoz, J. L. (1975) Application of fluor-hydroxyl exchange data to natural micas. (abstr.) Geological Society of America Abstracts with Programs, 7, 1179.

McCauley, J. W. and Newnham, R. E. (1971) Origin and prediction of ditrigonal distortions in micas. American Mineralogist, 56, 1626–1638.

Miijano, T. and Miijano, S. (1982) Ferri-annite from the Dales Gorge Member iron-formations, Wittenboom area, Western Australia. American Mineralogist, 67, 1179–1194.

Ramsay, C. R. (1973) Controls of biotite zone mineral chemistry in Archaean metasediments near Yellowknife, Northwest Territories, Canada. Journal of Petrology, 14, 467–488.

Robert, J. L. (1976a) Phlogopite solid solutions in the system K_2O–MgO–Al_2O_3–SiO_2–H_2O. Chemical Geology, 17, 195–212.

Robert, J. L. (1976b) Titanium solubility in synthetic phlogopite solid solutions. Chemical Geology, 17, 213–227.

Rousseaux, J. M., Laverde, C. G., Nathan, Y., and Rouxhet, P. G. (1973) Correlation between the hydroxyl stretching bands and the chemical composition of trioctohedral micas. Proceedings of the International Clay Conference (Madrid), 89–98.

Rouxhet, P. G. (1979) Hydroxyl stretching bands in micas: A quantitative interpretation. Clay Minerals, 8, 375–388.

Rutherford, M. J. (1973) The phase relations of aluminous iron biotites in the system $KAlSi_3O_8$–$KAlSiO_4$–Al_2O_3–Fe–O–H. Journal of Petrology, 14, 159–180.

Serratosa, J. M. and Bradley, W. F. (1958) Determination of the orientation of (OH) bond axes in layer silicates by infrared absorption. Journal of Physical Chemistry, 62, 1164–1167.

Shannon, R. D. (1976) Revised effective ionic radii and systematic studies of interatomic distances in halides and chalogenides. Acta Crytallographica, A32, 751–767.

Spear, F. S., Hazen, R. M., and Rumble, D., III (1978) Sodium trioctohedral mica from the Post Pond Volcanics, Vermont. Transactions, American Geophysical Union (EOS), 59, 1216.

Spear, F. S., Hazen, R. M., and Rumble, D. III (1981) Wonesite: a new rock-forming silicate from the Post Pond Volcanics, Vermont. American Mineralogist, 66, 100–105.

Stevens, R. E. (1946) A system for calculating analyses of micas and related minerals to end members. U.S. Geological Survey Bulletin 950, 101–127.

Strunz, H. (1970) Mineralogische Tabellan. Geest und Portig, Leipzig.

Takeda, H. and Ross, M. (1975) Mica polytypism: Dissimilarities in the crystal structure of coexisting 1M and $2M_1$ biotite. American Mineralgoist, 60, 1030–1040.

Tracy, R. J. (1978) High grade metamorphic reactions and partial melting in pelitic schist, west-central Massachusetts. American Journal of Science, 278, 150–178.

Tracy, R. J. and Robinson, P. R. (1978) Metamorphic isograd mapping in central Massachusetts and the study of changing mineral compositions in metamorphism. Geological Society of America Abstracts with Programs, 10, 89.

Vedder, W. (1964) Correlations between infrared spectrum and chemical composition of micas. American Mineralogist, 49, 736–767.

Vedder, W. and McDonald, R. S. (1963) Vibrations of the OH ions in muscovite. Journal of Chemical Physics, 38, 1583–1590.

Vedder, W. and Wilkins, R. W. T. (1969) Dehydroxylation and rehydroxylation, oxidation and reduction of micas. American Mineralogist, 54, 482–509.

Wilkins, R. W. T. (1967) The hydroxyl-stretching region of the biotite mica spectrum. Mineralogical Magazine, 36, 325–333.

Wones, D. R. (1963a) Phase equilibria of "ferriannite," $KFe^{2+}_3Fe^{3+}Si_3O_{10}(OH)_2$. American Journal of Science, 261, 581–596.

Wones, D. R. (1963b) Physical properties of synthetic biotites on the join phlogopite–annite. American Mineralogist, 48, 1300–1321.

Wones, D. R. and Eugster, H. P. (1965) Stability of biotite: Experiment, theory, and application. American Mineralogist, 50, 1228–1272.

Manuscript received, March 3, 1981;
accepted for publication, February 21, 1983.

Appendix

Analytical techniques

All of the data utilized in this study represent complete analyses for up to 14 elements (Na, Mg, Al, Si, K, Ca, Ti, Cr, Mn, Fe, Zn, Ba, F, Cl). Most of the analyses were performed at Caltech on an automated 3 spectrometer MAC-5 SAE electron microprobe interfaced to a DEC PDP-8/E minicomputer for control and on-line data reduction. Additional analyses were performed at Harvard on a 3 spectrometer ARL EMX-SM microprobe using KRISEL automation and interfaced to a DEC PDP-11/05 minicomputer for control and on-line data reduction. X-ray intensities were converted to oxide weight percentages by employing the methods of Bence and Albee (1968), and correction factors modified from Albee and Ray (1970). Operating conditions were 15 kV accelerating potential and 0.05 μA (CIT) or 0.02 μA (HU) sample current (on brass); a nearly identical set of simple oxides and silicates was used as primary standards in both laboratories. At CIT counting times ranged from 15–90 seconds and were controlled by the computer to yield precision of better than 1% for oxides with abundances of >1 wt.%, and better than 5% for oxides in the range of 0.1–1.0 wt.%. At HU, individual measurements were terminated after 30 seconds counting time or 60,000 accumulated counts, which results in a statistical precision similar to that achieved at CIT. Based on repetitive analyses of the same two internal standards in both laboratories, accuracy of the analyses is judged to be better than ~2% (relative) for major elements and 2–5% (relative) for minor elements (*cf.*, Champion *et al.*, 1975).